NASA TECHNICAL NOTE

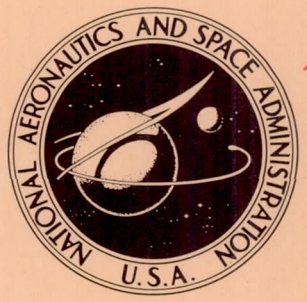

NASA TN D-1977

NASA TN D-1977

A MICROMETEOROID VELOCITY DETECTOR

by Frank Neuman
Ames Research Center
Moffett Field, Calif.
and Stanford University

NATIONAL AERONAUTICS AND SPACE ADMINISTRATION - WASHINGTON, D. C. - SEPTEMBER 1963

TECHNICAL NOTE D-1977

A MICROMETEOROID VELOCITY DETECTOR

By Frank Neuman

Ames Research Center
Moffett Field, Calif.

and

Stanford University

NATIONAL AERONAUTICS AND SPACE ADMINISTRATION

NATIONAL AERONAUTICS AND SPACE ADMINISTRATION

TECHNICAL NOTE D-1977

A MICROMETEOROID VELOCITY DETECTOR*

By Frank Neuman

SUMMARY

A feasibility study for a particular type of particle velocity detector is made. The detector considered consists of two light screens with known spacing. A particle penetrating the successive light screens scatters light which is detected by means of photomultiplier tubes. The time difference between the photomultiplier tube outputs is a measure of the particle velocity.

Such detectors have been used many times in free-flight wind tunnels. The question that is answered here is whether such a system is useful in space for detecting extremely small particles which have very high velocities and which arrive from unknown directions at random times with an unknown average rate. Can meaningful measurements be made in the presence of noise due to stray light? The answer is a qualified "yes."

---

*A thesis submitted in June 1963 to the Department of Electrical Engineering and the Committee on the Graduate Division of Stanford University in partial fulfillment of the requirements for the degree of Engineer.

INTRODUCTION

The hazard which micrometeoroids present to space vehicles was recognized long before the first man-made satellites were flown. For this reason all the early American and Russian satellites carried some type of meteoroid detectors (ref. 1). At present, with manned space flight in mind, a satellite has been planned for the sole purpose of obtaining more information on the particle environment in space (ref. 2). One can think of two types of experiments. In the first type, which may be called engineering experiments, one exposes surfaces of important structural materials such as aluminum and steel to the micrometeoroid environment and measures penetration rates as a function of material thickness. These experiments fulfill an immediate need for design information.

In the second type of experiments, which may be called scientific experiments, one attempts to obtain space environment information which, ideally, does not depend on the instrument used. In the case of micrometeoroids one would be interested in the spatial distribution, the variation of mass with abundance, and the velocity distribution; as well as density, velocity, and mass of individual micrometeoroids. So far the only operational instrument in the scientific class is the momentum detector which measures the product of mass and velocity of an impact. It is clear that if such an instrument could be coupled with a velocity or an energy detector, the more fundamental physical quantities of velocity and mass could be separated.

In one type of velocity measuring apparatus two plastic capacitor foils of known spacing were used (ref. 3). The particle must penetrate the foils and the time interval which elapses between the discharges of the two capacitors is a measure of the particle velocity. However, to prevent the particle's breakup and velocity reduction such foils must be extremely thin. This suggests that when very small particles at high velocities must be detected, a method of measurement is desirable which does not alter any parameter of the particle and which preserves the particle for further analysis. In this report the physical limitations of such an instrument will be investigated. To make an estimate of these limitations, all the available environmental information must be used.

From visual observations of meteors, radar measurements, rocket and satellite observations, a crude estimate of the spatial distribution of micrometeoroids has been made. For the purpose of this report only the data are of interest which help to determine the design parameters of the instrument. The most important piece of information is an estimate of the mass versus flux distribution of the meteoroid population. Figure 1 shows various estimates and measurements (ref. 4). The diagram vividly points out how much there is yet to learn. Other important pieces of information needed are the densities and the shapes of the cosmic dust particles. Data of this kind has been obtained by high altitude rocket studies (ref. 5). The measurements shown in figure 1 all have been momentum measurements. The data have been reduced

to mass by estimating an average particle velocity. At this time no measurements have been made which determine both velocity and momentum of individual cosmic dust particles.

The micrometeoroid velocity detector described in this report consists of three main types of components, the housing, the two light screens, and the four photo-multiplier tube detectors (fig. 2). From a specified field of view the instrument housing accepts micrometeoroids and it unavoidably accepts also an amount of undesirable light.

By proper geometrical design and use of a special black paint, an attempt is made to reduce stray light falling on the face of the photo-multiplier tube.

The light screens are rectangular beams of focused sunlight. Focusing is necessary to achieve the light intensity needed to detect the small size particles.

When a cosmic dust particle traverses the first light screen, light is scattered and reflected from the particle and a small fraction of this light reaches the cathode of the photomultiplier tube. The resulting current forms the start pulse of the detector. A similar output from the second screen forms the stop pulse, and the time elapsed between the two events is electronically measured. Since the distance between the screens is known, the time of flight between the screens determines the velocity of the dust particle. The addition of a momentum detector behind the light screens allows the determination of particle mass.

The principle of operation of the cosmic dust velocity detector is very simple. Still a surprising number of problems must be solved. Only a few of these are treated in detail in the following report which may be considered a feasibility study. For completeness, some of the problems not treated later are enumerated here. (1) The production of high-speed small particles for testing of the instrument has not been solved satisfactorily. (2) No consideration is given in this report to the actual circuit design. (3) Power, weight, and temperature control considerations in space are not treated. (4) The method of producing the light screens by proper focusing of the sunlight and the difficult problem of stabilizing the instrument to maintain this focus are not investigated.

SYMBOLS

a	width of the light screen
A_r	relative front window size, (number of particles passing through front screen per day)/(number particles striking a one m^2 area per day) (See fig. 1 for the denominator.)
C	photomultiplier tube load capacity
d	distance between light screens
e	electronic charge 1.602×10^{-19} coulomb
E	error rate of the velocity detector
E_{coll}	collection efficiency of the optical system, (number photons collected at one photo cathode)/(number photons scattered)

E_{quant}	quantum efficiency of the photomultiplier, (number electrons emitted from photo cathode)/(number photons collected at 1 photo cathode)
E_{scat}	scattering efficiency of the particle, (number photons scattered)/(number photons incident)
G	current gain of the photomultiplier tube
i	current, amperes
I	intensity magnification of the sun's energy
Ic	number of particles going through the circular area of radius r
K	proportionality constant
L	thickness of the light screen, through which the particle has to travel, cm
m	mean of a probability distribution
n	number of photons arriving at the photo cathodes of one light screen
n_1	average number of errors per second when 1 additional pulse occurs in the interval t_m
n_2	average number of errors per second when 2 additional pulses occur in the interval t_m
$\binom{n}{x}$	binomial coefficient, $\frac{n!}{x!(n - x)!}$
n_I	noise pulse rate from the first light screen
n_{II}	noise pulse rate from the second light screen

n_q number of light quanta arriving in the vicinity of the earth from the sun in the range from 2000 to 8000 Angstrom, 4.85×10^{16} (quanta/cm^2sec)

N_{av} collection rate, average number of micrometeoroids being detected per day

N_e average number of electrons required from the photo cathode to get a high probability of an output distinguishable from noise, electrons

$P(.)$ probability density function

$P(y/x)$ probability that event y will occur given that event x has occurred

q charge, coulomb

r equivalent radius of a particle, cm

R resistance, ohms

R_d phototube distance from a point source of light, cm

R_c coincidence rate, (number of particles going through both screens per day)/(number of particles going through front window only)

v velocity of the particle, cm sec^{-1}

t_m maximum flight time of a particle through a light screen, sec

T_m maximum flight time of a particle between light screens, sec

$\hat{V}$ peak voltage of a photomultiplier output pulse due to one primary electron, volts

x number of primary electrons due to n photons

y minimum number of output pulses to be considered an event

Z standardized normal variable

α,β direction angles, defined in figure 5

α average number of noise pulses per second

μ target size reduction factor

σ variance

$d\Sigma$ differential solid angle

τ pulse width

Φ influx rate, number of micrometeoroids above the detection threshold striking a 1 m^2 area per day (See fig. 1.)

Φ_o light flux from a zero magnitude photovisual star, 2.43×10^{-10} lumen cm^{-2}

Φ_T total starlight flux through a unit area, lumen cm^{-2}

THE SENSITIVITY OF THE MICROMETEOROID VELOCITY DETECTOR

The power of resolution of the micrometeoroid detector is defined as the minimum equivalent particle radius that the instrument can detect with some certainty. The equivalent particle radius is the radius of a circle which has the same area as the projected area of the micrometeoroid (see fig. 3). The degree of certainty of detection that is desired depends on the number of particles which traverse the instrument. For instance, if several hundred particles above a certain size traverse the instrument, 80-percent detection would be sufficient to infer as to the total number of particles which actually did traverse the instrument. The design of the transducer, which includes the light screen, the light collector, and the photomultiplier, offers the most serious limitation to the size of the particle that may be detected with any degree of certainty.

If the previously defined quantities are used, the equation for minimum detectable particle size will look as follows:

$$r(\text{cm}) = \left(\frac{1}{\pi} v \frac{1}{L} \frac{1}{n_q} \frac{1}{I} \frac{1}{E_{scat}} \frac{1}{E_{coll}} \frac{1}{E_{quant}} N_e\right)^{1/2} \qquad (1)$$

By writing a unit equation the above equality may easily be checked. The individual factors of this equation will now be discussed further.

A diagram of the detector's light screen arrangement is shown in figure 2. The thickness of the light screen, L, through which the particle has to travel is limited by the size of the instrument and also by the requirement that stray light must be kept to a minimum, since stray light constitutes noise. The velocity range of the particles is estimated from the following astronomical constants. The escape velocity from the surface of the earth is 11 kilometers per second. This would be the lowest velocity one would expect cosmic dust to have in the vicinity of the earth. The highest velocity of micrometeoroids expected is 72 kilometers per second. This figure is derived from the following constants. The escape velocity from the sun's gravitational field at one astronomical unit is 42.2 kilometers per second while the earth velocity around the sun is 29.8 kilometers per second. Hence, the maximum collision velocity of a micrometeoroid bound to the solar system with the earth would be 72 km sec^{-1}. Particles with speeds greater than 72 km sec^{-1} have velocities of hyperbolic orbits. Such particles are not likely to be intercepted as they are probably smaller in number. Satellite motions with respect to the earth have been

neglected in the above discussion. They will increase further the expected spread of velocities.

A great amount of theoretical information is available on light scattering of spherical particles of different sizes and different indexes of refraction. No theory, however, exists for light scattering of irregular shaped small particles. One thing that can be learned from the plotted scattering distributions for small spherical particles is that the intensity for different scattering angles will vary widely with wavelengths (ref. 6). This points out the fact that it would be undesirable to use single frequency light as that of a laser, for instance, even though the use of a single frequency light could provide a method for keeping stray light from the detector by filtering the incoming light to the phototube. The relatively wide band width that sunlight provides helps to randomize the scattering angles and thus makes the photons arriving at the photo-cathode more likely proportional to the actual projected area of the particle.

In June 1961, the Venus Fly Trap experiment actually sampled micrometeoroids from an altitude of 88 to 168 kilometers above the earth surface (ref. 5). Basically, three types of micrometeoroids were found; nearly spherical particles of 2 to 3 microns in diameter, irregular specimens which almost have the appearance of museum meteorites except for their smallness, and extremely irregular pieces of fluffy material. The regular spheres comprised the smallest percentage of micrometeoroids found in this experiment. For this reason not much more can be done than to estimate the percentage of photons scattered and to assume uniform scattering.

As equation (1) shows, the greater the photon flux in the light screen, the greater the sensitivity of the velocity detector. To provide the intense light which is needed to get a reasonable detector sensitivity it is most economical to use focused sunlight directly. Using 10-percent efficient solar cells and 10-percent efficient light sources would give an over-all efficiency of only 1 percent, while with a mirror collection system a much higher efficiency can be achieved. The difficulty with using mirrors, however, is that very precise attitude control on the light collecting apparatus must be maintained. This calls for a complex instrument; however, the use of such an instrument is not ruled out as satellites get bigger and more sophisticated.

The collection efficiency of the velocity detector is a function of its geometry. For a very simplified model of the telescope and its input see figure 4. The micrometeoroid is a point source radiating equally in all directions, and the photocathode of the phototube is a distance R_d away from the point source. Then the intensity of light falling onto the photocathode is proportional to $1/R_d^2$. From this point of view it is clear that it would be desirable to have the photomultiplier tube as close to the micrometeoroid as possible. However, there are two more considerations. Light from various sources enters through the same opening through which micrometeoroids enter the instrument. This light constitutes noise. Also, the closer the photocathode is to the light screen, the greater are the variations in telescope sensitivity as function of the point through which the micrometeoroid penetrates. Figure 4 shows a better detection uniformity when two phototube outputs are paralleled.

Three principal sources of disturbing light are present: starlight, moonlight, and earthlight. The telescope is assumed to be protected against sunlight since its collection mirror must always be sun oriented. Therefore, the mirror shields the telescope from the direct rays of the sun.

The data for the following calculations are taken from reference 7. Starlight from the whole sky is equivalent to 490 zero photo-visual magnitude stars (ref. 7). If the total light flux is assumed to be equally distributed over the whole sphere (isotropic field), the light flux going through one side of a flat surface of 1 cm^2 in one direction will be

$$\Phi_T = \frac{1}{4} 490\Phi_o = 2.98\times10^{-8} \text{ lumen } cm^{-2} \qquad (2)$$

Total number of quanta due to starlight through 1 cm^2 = 2.98×10^{-8} lumen cm^{-2} 4.12×10^{15} quanta sec^{-1} $lumen^{-1}$ = 1.23×10^{8} quanta sec^{-1} cm^{-2}.

Satellites are close to the earth in relation to the earth-moon distance. The illumination at earth's surface due to full moon is 3×10^{-6} that of the sun (ref. 8). The sun radiates 4.85×10^{16} quanta cm^{-2} sec^{-1}, the moon $4.85\times10^{16}\times3\times10^{-6}$ = 1.455×10^{11} quanta cm^{-2} sec^{-1}; that is, moonlight at full moon is about 1000 times as strong as starlight.

The Bond Albedo is the ratio of total light reflected from a sphere to total light incident on it (ref. 7). The earth and moon albedo are: earth = 0.34, moon = 0.07. From these figures it is obvious that for a satellite in the vicinity of the earth, the earthlight is the strongest contributing factor to noise due to stray light.

Which type of light we must guard against depends on the mission that is flown. On earth satellites, all three sources of light are important. If the design is such that only noise due to starlight is small enough not to cause an excessive amount of errors, one can guard against moonlight and earthlight by not pointing the instrument in the direction of the moon or the earth. For space probe missions only starlight and sunlight need to be considered. To prevent operation under unfavorable conditions the output pulses of the photomultiplier tube from the first light screen of the detector can be counted. When the counting rate goes too high, indicating a noise condition against which the coincidence circuits cannot discriminate, the velocity detector will be disabled. Also, the noise pulse count can be telemetered to ground at all times as an indication of confidence for the recorded data.

The characteristics of the phototube detector and the quantum nature of light will offer the most severe limitations to the detection. To design an optimum detection system, the characteristics of the phototube must be clearly understood. Therefore, a later section of this report is devoted to that topic. At this time, let us state briefly that a detection system is needed which can distinguish the least possible number of photons falling on the photocathode as an input as compared to random thermal and starlight noise. These requirements indicate a phototube with a low thermal emission and a high quantum efficiency, and an electronics detection system following the phototube which recognizes a minimum number of primary electrons as a signal output.

GEOMETRIC FACTORS DETERMINING THE USEFULNESS OF THE MICROMETEOROID VELOCITY DETECTOR

Even with coincidence circuitry, due to noise, a certain number of false particle counts will be made. This noise counting rate must be at least an order or magnitude lower than the actual particle rate. Hence, an estimate of the number of particles that will be encountered must be made to determine whether a certain size velocity detector is of practical use.

Then

$$N_{av} = A_r R_c \Phi \text{ (counts per day)} \tag{3}$$

where the quantities A_r and R_c must be calculated from the geometry of the detector and Φ must be estimated from figure 1.

It is intuitively clear that in an isotropic field, A_r must be equal to the ratio of the respective areas

$$A_r = \frac{\text{area of the front screen}}{\text{area of the reference surface}} \tag{4}$$

Also, this value should not depend on the shape of the screen. To calculate the average error in velocity measurement one must also know the directional pattern of the screen surface as a function of the angle α. We will obtain this information by first considering the circular front window of figure 5(a).

The average number of particles arriving from a solid angle is proportional to the magnitude of the solid angle. Hence, $d\Sigma$, the differential flux from direction α (for $\beta = 0$ to 2π) is

$$d\Sigma = K2\pi r^2 \sin \alpha \, d\alpha \tag{5}$$

Viewing the front window from an angle α it appears as an ellipse and its target size is reduced by a factor

$$\mu = \frac{\pi r^2 \cos \alpha}{\pi r^2} = \cos \alpha \tag{6}$$

Therefore the average number of particles arriving at the screen from a direction α is

$$d[I_c(\alpha)] = \mu \, d\Sigma = K2\pi r^2 \sin \alpha \cos \alpha \, d\alpha \tag{7}$$

Then the total flux is

$$I_c = \int_{\alpha=0}^{\pi/2} \mu \, d\Sigma = K\pi r^2 \tag{8}$$

which is proportional to the area of the screen as was expected.

We must now generalize to other surfaces. Figure 5(b) shows an area and two different projections of the same area viewed from an angle α for two different angles β. See figure 5(a) for the definitions of the angles. Since in each case the respective differential areas are multiplied by a constant factor $\cos \alpha$, the size of the projected area is independent of the angle β, even though its shape varies widely.

$$A_2 = A_3 = A_1 \cos \alpha \tag{9}$$

We are now prepared to generalize. Taking the results from equations (8) and (9) one can see that (4) holds for any shape of screen.

The expression of equation (7) can be normalized by dividing through by the proportionality constant and the area of the screen.

$$\frac{d[I_c(\alpha)]}{K\pi r^2} = 2 \sin \alpha \cos \alpha \, d\alpha \tag{10}$$

We rewrite equation (10) by use of trigonometrical identities and define it as

$$p(\alpha)d\alpha \triangleq \sin 2\alpha \, d\alpha \tag{11}$$

The expression $p(\alpha)$ of equation (11) can be thought of as a probability density function since the isotropic field is of statistical nature, and

$$\int_{-\infty}^{\infty} p(\alpha)d\alpha = 1$$

From equation (9) $p(\alpha)$ is the probability density function for any flat surface (see fig. 6). This indicates that on the average only 3 percent of all particles arrive from angles between 0 - 10° (from the front), while 17.5 percent will arrive from angles between 40° - 50°. The relative flux intensity on a surface is redrawn in figure 7 in polar coordinates to show the directional pattern of a flat surface. The result is, at first glance, somewhat surprising since one would expect $\alpha = 0^\circ$ to be the favored direction (μ is a maximum at $\alpha = 0$). However, the differential flux is a function of $d\Sigma$ also, which has its maximum at $\alpha = \pi/2$.

By adapting the method used in reference 9, the coincidence ratio was calculated for light screens with a cubic geometry. A value of 0.213 was obtained for R_c. This problem actually involves quadruple integration, resulting in a rather lengthy method when one intends to

investigate various detector geometries. For these reasons it is useful to have an experimental technique to measure the coincidence ratio directly.

The basic difficulty lies in simulating an isotropic field of particles. This was solved by an experimental analog and no mathematical proof is given.

A 5.25-inch radius plastic hemisphere was spray painted white inside and outside to get good light diffusion. The opening simulating the front screen was placed at the center of the hemisphere, and was made much smaller than the radius of the hemisphere. This limits the variation in light intensity on any point of the screen due to illumination from a particular spot of the sphere's surface. The remaining error is largest when the light comes from a direction close to the plane of the front screen, but this effect is minimized due to the smaller projected area of the screen.

The hemisphere is inserted into a large box painted white on the inside (see fig. 8) where ten small light bulbs are distributed to illuminate the sphere with approximately equal intensity from all directions.

The rest of the system is explained in figure 8. The variac is used to increase the light intensity as the distance between front screen and back screen is increased in order to stay above the noise level of the tube. At points where the light intensity is increased, two measurements must be made.

The coincidence ratio is simply the ratio of photomultiplier output voltage measured at distance d (corrected by any light increase factors) to the voltage measured when d = 0.

The results are plotted in figure 9. The result for d = a which was computed earlier is very close to the measured value. Notice the rapid decrease in coincidence ratios for small separations between screens. As d increases further, the front face appears as a point source and further decrease of light intensity versus distance is proportional to $1/d^2$.

Several geometric arrangements of the telescope can be investigated, including a shield of some sort which will be needed to keep out starlight and reduce the noise background. One type of shield is shown in figure 10(b). Less particles than shown in figure 10(a) will now go through the front screen, but the number of particles going through the back screen have not been reduced since the shield does not cut off any coincident rays. Hence, the collection rate of coincident particles can be computed as if the shield were absent. The computation would not indicate, however, the reduction of particle flux through the front window. If this is of interest, special measurements must be made.

Figure 10(c) shows a straight shield. Obviously this type of shield reduces the number of coincident particles captured when compared to figure 10(a). See table I for a comparison of the performances of the different detector geometries.

The above method can be extended to find the acceptance pattern of any velocity detector configuration by the simple method of masking

different parts of the hemisphere and recording the percentage of light received from the unmasked portion of the hemisphere. The acceptance pattern must be known for two purposes, to determine the errors in velocity measurement because the particle does not traverse the shortest flight path, and to determine the direction of the measured micrometeoroid flux.

PHOTOMULTIPLIER TUBE CONSIDERATIONS

In the micrometeoroid velocity detector we are looking at small particles passing a 1-centimeter illuminated distance at speeds between 7 and 72 kilometers per second. Hence, the duration of events to be detected ranges from 0.14 to 1.4 microseconds. From equation (3) and figure 1 using Whipple's data, it is estimated that on the average about four particles of a 2-micron radius would be detected per day. The same instrument would detect on the average a 100-micron particle every 1000 hours. This indicates that to get a statistical sample the photomultiplier tube must be used in an optimum fashion to detect a minimum number of photons arriving at the photocathode. Since the large gain of the tube makes it possible to distinguish 1 photoelectron, it becomes necessary to investigate the noise behavior of the tube very carefully (ref. 10).

To understand noise behavior of a tube, the gain of the tube must be known. Measurements were made with an EMI9502B* tube which has the following nominal characteristics: For an over-all voltage of

---

*Electrical and Musical Instrument Co., Los Angeles, Calif.

1500 volts across a uniform dynode chain it has a sensitivity of 2000 amperes per lumen. From this information the current amplification can be estimated:

$$G = \frac{2000 \frac{\text{amp}}{\text{lumen}} \; 0.624\times10^{10} \text{ electron/sec amp}}{4.53\times10^{15} \frac{\text{quanta}}{\text{sec lumen}} \; 0.1 \frac{\text{electron}}{\text{quantum}}} = 2.75\times10^{7} \qquad (12)$$

Another way of arriving at an approximate value of current amplification is found by estimating the dynode multiplication factors. These are equal to 6 for the amplification from the photocathode to the first dynode and equal to 4 between all other dynodes. Hence, for the 13-dynode tube we calculate:

$$G = 6\times4^{12} \approx 10^{8}$$

Since the approximate gain of the tube was known, the actual tube gain was measured more easily (see fig. 11).

Figure 12 shows a circuit to measure the dark current pulse rate. The usual calculation for the mean pulse height is

$$\hat{V}_{ideal} = \frac{q}{C} = \frac{Ge}{C} \qquad (13)$$

For figure 12

$$\hat{V} = \frac{3.3\times10^{7}\times1.6\times10^{-19}}{11.5\times10^{-12}} = 0.46\text{v}$$

This assumes a current impulse is delivered, so that current through the resistor during the charging of the capacitor is negligible. When this is not the case, the pulse height will be lower than that calculated

above. Figure 13 shows a Gaussian current pulse. For this actual pulse shape it is difficult to calculate the output voltage. Therefore, let this pulse be roughly approximated by a rectangular pulse having the same total charge, and a width equal to the half-amplitude time spread ($i = q/\tau$). Then the actual peak output voltage for a pulse is reduced by a factor

$$\frac{\hat{V}_{actual}}{\hat{V}_{ideal}} = \frac{RC}{\tau}\left(1 - e^{-\tau/RC}\right) \qquad (14)$$

due to the presence of resistance. In figure 14 the relationship of equation (14) has been plotted. It shows that for a given load capacitance the pulse height increases with increased load resistance.

For the EMI9502B with a load as shown in figure 15,

$$\frac{RC}{\tau} = \frac{11.5\times10^{-9}}{18\times10^{-9}} = 0.64$$

$\hat{V}_{actual} = \hat{V}_{ideal}(RC/\tau)(1 - e^{-\tau/RC}) = 0.46\times0.64\times0.98 = 0.293$ volts is the average output pulse height due to 1 photoelectron. This value has been used as a scale in drawing the abscissa of figure 15.

Since thermal electron emission is not a function of supply voltage, the quantity eG is useful as the scale for the abscissa because figure 15 remains the same even when the tube gain is altered by changing the supply voltage. To obtain an estimate of the proportion of pulses originating at the photocathode, the photocathode was reverse biased by 100 volts. The pulse rate for small pulses (0.33 eG) decreased by

a factor of 10, and the pulse rate for larger pulses (0.66 eG) decreased by a factor of 150. Hence, nearly all large pulses originate at the photocathode, which is not a surprising result.

When coincidence methods are to be used to reduce counting errors, it is important to know the time distribution of the pulses (ref. 11). Figure 12 shows the equipment required to measure this distribution. CRO II was free running at a known speed and the scope face was masked except for 1 centimeter of height. For each pulse above a minimum height CRO I swept once and applied a pulse to the slow sweeping CRO II. A photograph of the face of CRO II is shown in figure 16. By considering the last event of the first row identical with the first event of the next row (even though they are not) we have a relatively long sample of pulse versus time distribution.

One can now test for the assumption that the pulses form a Poisson time distribution. This is a reasonable assumption to be tested since such a distribution will result provided the following conditions hold:

1. The probability that n electrons are emitted within the interval $(t_o, t_o + t)$ is independent of the starting time t_o.

2. For an infinitesimal interval of length, Δt, the probability that 1 electron occurs within Δt is proportional to Δt, and the probability that more than 1 electron occurs within Δt is negligible.

3. The time of emission of individual electrons within intervals that do not overlap is statistically independent.

Then the probability of exactly n electrons being emitted in the interval t is:

$$P_n = P(n \text{ electrons in the interval } t) = \frac{(\alpha t)^n}{n!} e^{-\alpha t} \qquad (15)$$

where αt is the average number of pulses in the interval t.

One can now count the number of pulses in figure 16 to determine the average number of pulses per second. By dividing figure 16 into intervals of length $t = 1/\alpha$, one can count the number of pulses in each interval and make a table of their distribution. See table II and note the agreement between theoretical and measured values.

Environmental temperature drastically affects the noise output of the tube. With decrease in temperature the photomultiplier tube gain remains virtually unchanged, while the noise pulse rate is divided in half for every 10° C temperature decrease. Therefore, pulse height versus pulse rate was measured again when the tube was cooled to -50° C and it was found that the Poisson law still applied.

What does this mean in terms of the micrometeorite detector? If the maximum temperature at which the tube would work on the satellite is known, the pulse height distribution of the tube for this temperature can be measured, and the one parameter noise statistics of the tube would be completely described.

Unfortunately, when the photomultiplier tube is integrated as part of the micrometeoroid detector, light from the stars will arrive at the photocathode and thus constitute noise. At first glance, it seems that this light should cause a steady-state dc value. However, for very weak light inputs, this is not so.

To determine experimentally what happens, the tube was placed in a container which was designed to let in a minimum amount of starlight and still allow the system to perform as a micrometeoroid velocity detector (see fig. 2). The instrument and its associated measuring equipment were set up on Mount Hamilton, California, during the new-moon period in August 1962. The experimental set-up is shown in figure 17.

The results of the experiment are illustrated in figures 18, 19, and 20. As figure 18 shows, the pulse shape due to the starlight noise is identical with that of thermal noise alone. However the frequency of the noise pulses increased by 1-1/2 decade (fig. 19). With such an increase, extreme cooling of the phototube would give rise to little improvement in the over-all performance of the detector. It is hoped, however, that eventually a considerable reduction in noise due to starlight could be achieved by more careful experimental design of the "black-box" structure.

The statistical characteristics of the noise pulses were tested by the same method as described earlier and were found also to be Poisson (see fig. 20). This follows because the addition of two Poisson processes will result in another Poisson process with a new parameter α being the sum of the two individual parameters.

THE SYSTEM

In a detector two types of errors can be made. The velocity of a micrometeoroid going through both light screens would not be measured as a result of the failure of an output from at least one of the light

screens (this is called a type I error); or, as a result of the noise, both screens could give an output in the proper sequence when actually no event has taken place (this is called a type II error). Designing the experiment to minimize one type of error will necessarily increase the probability of the other type of error; therefore, an acceptable compromise must be found. The object is to count a large proportion of all particles entering the detector and to get an average error count of only a few percent of the actual count rate.

Errors of type I are estimated in the following manner. Let n be the number of photons arriving at the photocathode, and p be the quantum efficiency of the phototube. Then the probability that exactly x photoelectrons are emitted from the photocathode is a binomial distribution (ref. 12)

$$p(x) = \binom{n}{x} p^x (1 - p)^{n-x} \tag{16}$$

with mean and variance

$$m = np \tag{17}$$

$$\sigma = \sqrt{np(1 - p)} \tag{18}$$

For small p (10 percent) and large n the binomial probability distribution can be approximated by the normal distribution with the same mean and variance. The evaluation using the normal distribution approximation can be shown to be (ref. 13)

$$P(x') \approx P_{r_N}\left[\frac{\left(x' - \frac{1}{2}\right) - m}{\sigma} < \frac{x - m}{\sigma} < \frac{\left(x' + \frac{1}{2}\right) - m}{\sigma}\right]$$

$$= P_{r_N}\left[Z \leq \frac{\left(x' + \frac{1}{2}\right) - m}{\sigma}\right] - P_{r_N}\left[Z \leq \frac{\left(x' - \frac{1}{2}\right) - m}{\sigma}\right] \qquad (19)$$

where the values of the standardized normal variable

$$P_{r_N}(Z \leq Z') = \frac{1}{\sqrt{2\pi}} \int_{-\infty}^{Z'} e^{-Z^2/2}\, dZ \qquad (20)$$

can be determined from standardized normal tables.

It was shown earlier that only one-tenth of the pulses which are smaller than one-third of the average output pulse height originates at the photocathode. This indicates that one can reduce type I errors considerably by biasing the pulse discrimination circuits that follow the phototube output. To suppress virtually all pulses not originating at the photocathode, the discrimination circuits may be biased to distinguish pulses greater than $(1/2)eG$. The probability that the number of output pulses N is greater than or equal to y given that x primary electrons are present is

$$P(N \geq y/x) = \sum_{S=y}^{N} \binom{x}{S} \left(\frac{1}{2}\right)^{S} \left(\frac{1}{2}\right)^{N-S}$$

$$= \left(\frac{1}{2}\right)^{N} \sum_{S=y}^{N} \binom{x}{S} \qquad (21)$$

Since the processes expressed in equations (19) and (21) are independent, then (ref. 10)

$$P(x,N \geq y/x) = P(x)P(N \geq y/x) \tag{22}$$

Thus the probability of an output when n photons arrive at the photocathode is

$$P_{output} = \sum_{n=y}^{n} P(x)P(N \geq y/x) \tag{23}$$

This sum can easily be evaluated for a different number of incoming photons n and for a different minimum number of output pulses y which are considered an event. A sample calculation is shown in table III. Before discussing the significance of these figures let us estimate type II errors.

To reduce type II errors, coincidence methods are usually used when outputs from separate detectors are involved (ref. 10). However, delayed coincidence can also be applied when successive outputs from a single detector concerns us.

One can assume the following circuit. It gives an output pulse when, after an initial pulse, a minimum number of additional pulses occur within a given time. This time is chosen as t_m the maximum flight time of a particle in the light screen.

As previously shown the noise pulses occur according to the Poisson distribution

$$P_n(t_m) = P_n(n \text{ noise pulses in the interval } 0 \leq t \leq t_m)$$

$$= \frac{(\alpha t_m)^n}{n!} e^{-\alpha t_m} \tag{24}$$

where α is the average number of photomultiplier noise pulses per second. After each pulse the circuit counts for t_m seconds if the specified minimum number of pulses occur, for example, one extra pulse:

$$\begin{aligned} P_n(n \geq 1 \text{ in } 0 \leq t \leq t_m) &= 1 - P(0) \\ &= 1 - e^{-\alpha t_m} \\ &\approx 1 - (1 - \alpha t_m) \quad \text{for } \alpha t \ll 0.1 \\ &= \alpha t_m \end{aligned} \tag{25}$$

or two extra pulses

$$\begin{aligned} P_n(n \geq 2 \text{ in } 0 \leq t \leq t_m) &= 1 - P(0) - P(1) \\ &= 1 - e^{-\alpha t_m}\left[\frac{\alpha t_m{}^0}{0!} + \frac{(\alpha t_m)'}{1!}\right] \\ &\approx 1 - (1 - \alpha t_m)(1 + a t_m) \\ &= (\alpha t_m)^2 \end{aligned} \tag{26}$$

There are an average of α counting intervals per second; hence, the probability that in these α counting intervals an event is indicated falsely is

$$\alpha P(n \geq 1) = \alpha(\alpha t_m) = \alpha^2 t_m = n_1 \tag{27}$$

$$\alpha P(n \geq 2) = \alpha(\alpha t_m)^2 = \alpha^3 t_m{}^2 = n_2 \tag{28}$$

where n_1 and n_2 are the average number of errors per second; for example, α = 1000 pps, t_m = 2μsec

$$n_1 = (1000)^2\ 2\times10^{-6} = 2 \text{ errors per sec}$$

$$n_2 = (1000)^3\ 4\times10^{-12} = 4\times10^{-3} \text{ error per sec}$$

In the above circuit it was assumed that the individual noise pulses are short when compared to t_m. A 0.1μsec pulse can reasonably be achieved, and indeed $t_m = 2\mu\text{sec} \gg 0.1\mu\text{sec}$.

Clearly a single coincidence circuit with $P_{\alpha_1}(n \geq 1)$ or even $P_{\alpha_2}(n \geq 2)$ cannot sufficiently reduce the effect of noise, when rare events must be detected (10-200 events per day). To reduce type II errors further, another coincidence arrangement which involves both screens can be employed. Again, the front screen must first indicate an event; therefore, the equation for noise improvement is identical with that previously developed.

Figure 21 shows that a 20μsec pulse is applied to the coincidence gate every time the first screen gives an output. This allows a maximum flight time between screens of 20μsec and slower particles will not be detected. From the second screen a 2μsec pulse is sent and checked for coincidence. In terms of the noise in the detectors this results in the following:

$$E\left(\frac{\text{errors}}{\text{seconds}}\right) = T_m n_I n_{II} \tag{29}$$

where n_I and n_{II} are the noise pulse rates from the first and second screens. Since $T_m = 10t_m$ (the screen distance is 10 times the screen thickness), the following holds

$$E = 10t_m n_I n_{II} \tag{30}$$

Two cases have been considered which resulted in n_1 and n_2 errors per second (eqs. (27) and (28)).

If noise pulse rates are assumed to be equal for both velocity screens, then the first case (eq. (30)) will become

$$E = 10t_m^3\alpha^4(\text{sec}^{-1}) \tag{31}$$

which gives

$$\alpha = \sqrt[4]{\frac{E}{10t_m^3}} = 1.06\times10^4\sqrt[4]{E} \tag{32}$$

For the second case

$$E = 10t_m^5\alpha^6(\text{sec}^{-1}) \tag{33}$$

which gives

$$\alpha = \sqrt[6]{\frac{E}{10t_m^5}} = 3.82\times10^4\sqrt[6]{E} \tag{34}$$

The permissible noise pulse rates for one error per week and one error per month are shown in table V. It clearly shows the superiority of the second method.

A block diagram can now be drawn and the choice of logic circuitry justified (see fig. 22). For performance calculations the following assumptions are made:

1. If the geometry in figure 22 is used, starlight will contribute to the tube noise to give a maximum number of pulses of 2000 per second per tube.

2. Tubes are operated at -50° C. At this temperature the 2-inch diameter photocathode will emit about 6 thermal electrons per second, which is a negligible amount compared to starlight noise.

3. Output pulse length from one photoelectron (noise or signal) is 0.1μsec for both tubes in parallel monitoring the same light screen.

4. Sunlight in the light screen is intensified by a factor of 100.

5. Particles scatter photons equally over 4π steradians for the calculation of collection efficiency.

6. Scattering efficiency of the particles is 10 percent.

7. Average particle velocity is 15 km/sec (from Whipple).

8. Phototube quantum efficiency is 10 percent.

9. Particle influx rate follows the curve given in reference 4 and figure 1. (This curve gives a higher influx rate for small particles when compared to Whipple's 1957 data.)

10. Three output pulses within 2μsec from one phototube pair are considered an event.

Calculated Performance Data

1. The probability of detecting the smallest size particle considered is 78 percent (see table IV).

2. The equivalent radius of the smallest particle seen with the above reliability is from equation (1).

$$r = \left(\frac{1}{\pi} v \frac{1}{L} \frac{1}{n_q} \frac{1}{I} \frac{1}{E_{scat}} \frac{1}{E_{coll}} \frac{1}{E_{quant}} N_e\right)^{1/2}$$

$$= \left(\frac{1}{\pi} 1.5\times10^{6} \frac{1}{1} \frac{1}{4.85\times10^{10}} \frac{1}{10^{2}} \frac{1}{10^{-1}} \frac{1}{1.8\times10^{-2}} \frac{1}{10^{-1}} 10\right)^{1/2}$$

$$= 0.73 \text{ micron}$$

Above this size the probability of detection rapidly approaches 1. Below this size the probability of detection rapidly approaches zero. This can be verified by the method of calculating type I errors.

3. From equation (3) and figure 1 (McCracken), the average number of 2.5-micron particles counted per day in the vicinity of the earth is

$$N_{av} = A_r R_c \Phi$$

$$= \frac{1}{100}\ m^2\ 0.2\ 1\ \frac{\text{particle}}{m^2 - \text{sec}}$$

$$= 1\ \frac{\text{particle}}{500\ \text{sec}} = 182\ \frac{\text{particles}}{\text{day}}$$

(Whipple's estimate would result in a figure of $N_{av} = 4.4$ particles per day.)

4. From equation (33) the average number of errors due to noise is

$$E = 10(2\times10^{-6})^5(2\times10^3)^6$$

$$= 2\times10^{-8}\ \frac{\text{errors}}{\text{second}}$$

$$= 1 \text{ error in } 0.63 \text{ year}$$

This error rate is negligible, but one must consider the fast increase of errors as noise pulses increase (see table V) and be aware that the margin is not as great as it seems. Further improvement can be achieved by integrating the momentum detector into the coincidence scheme.

CONCLUDING REMARKS

It appears that special techniques would be required in order to achieve detection of micron-sized particles by light screens. The suggested method involves the sensing of pulses due to individual electrons originating at the photocathode of a photomultiplier tube. The analysis of the two basic types of errors, failure to detect a particle, and erroneously interpreting noise as a particle shows that a coincidence type of detection scheme can make the latter type of error reasonably small. Even after going to these lengths to avoid errors due to noise, an extremely intense light (of the order of 100 times the intensity of direct sunlight) would be required. This need for high intensity light screens may well be the deciding factor as to the practicability of the device for use in a space vehicle.

The suggested method of detection and noise discrimination in which the pulses resulting from individual electrons originating from the photocathode are scrutinized is believed to be new and may have wider application. For example, it might be applied to scintillation counters for the detection of extremely low-level rare nuclear events. The analog method used to investigate the directivity and coincidence ratio of the velocity detector should also be useful for other types of detectors.

Ames Research Center
National Aeronautics and Space Administration
Moffett Field, Calif., May 9, 1963

REFERENCES

1. Barber, Edda, and Sweitzer, Dorothy I.: Micrometeorites, High Velocity Impact Studies, and Problems of Space Travel Relating to Particle Impact. Literature Search no. 143, JPL, Oct. 15, 1959.
2. Hastings, Earl C., Jr.: The Explorer XVI Micrometeoroid Satellite - Description and Preliminary Results for the Period December 16, 1962, Through January 13, 1963. NASA TM X-810, 1963.
3. Goettelman, R. C., Softky, S. D., Arnold, J. S., and Farrand, W. B.: The Meteoroid and Cosmic-Ray Environment of Space Vehicles and Techniques for Measuring Parameters Affecting Them. Stanford Research Institute, Feb. 1961, WADD TR 60-846.
4. McCracken, C. W., and Alexander, W. M.: The Distribution of Small Interplanetary Dust Particles in the Vicinity of the Earth. NASA TN D-1349, 1962.
5. Anon.: Micrometeorite Collecting with a High-Altitude Rocket. American Astronomers Report. Sky and Telescope, Feb. 1962, pp. 84-5.
6. Cadle, R. D.: Particle Size Determination. Interscience Pub., Ltd. (London), 1955.
7. Allen, C. W.: Astrophysical Quantities. Athlone Press (London), 1955.
8. Anon.: Reference Data for Radio Engineers. Fourth ed., International Telephone and Telegraph Corp., N. Y., 1956.
9. Newell, Homer E., Jr.: Geometric Factors Underlying Coincidence Counting with Geiger Counters. Review of Scientific Instruments, vol. 19, no. 6, June 1948, pp. 384-89.

10. Engstrom, Ralph W.: Multiplier Photo-Tube Characteristics: Application to Low Light Levels. Jour. of the Optical Society of America, vol. 37, no. 6, June 1947, pp. 420-31.

11. De Benedetti, S., and Findley, R. W.: The Coincidence Method. Vol. 45 of Handbuch der Physik, Springer-Verlag (Berlin), 1958, pp. 222-259.

12. Parzen, Emanuel: Modern Probability Theory and Its Applications. John Wiley and Sons, Inc., N. Y., 1960.

13. Fraser, D. A. S.: Statistics - an Introduction. John Wiley and Sons, Inc., N. Y., 1958.

TABLE I.- VELOCITY DETECTOR PERFORMANCE COMPARISON WHEN A SHIELD IS USED ASSUMING THAT ON THE AVERAGE 17 PARTICLES WILL ENTER A 10- BY 10-CENTIMETER AREA PER DAY

Type of screen	2-micron particles entering front screen/day	2-micron particles entering both screens/day	$R_c{}^1 = \frac{\text{column}^3}{\text{column}^2}$
Fig. 10(a) (no shield)	17.0	3.76	0.22
Fig. 10(b) $d_2 = d_1$**	9.4*	3.76	.4
Fig. 10(c) d_3 = 5 cm	8.5	1.88	.22
Fig. 10(c) d_3 = 10 cm	3.76	1.1	.29

*Measurement by testing a model shield
**a = 10 cm, d = 10 cm

Note: If $R_c{}^1$ is used in calculating the number of micrometeorites counted per day on the average, the flux rate φ must be reduced to φ^1 accounting for the effect of the shield. That this must be done is clear because the detectors of figures 10(a) and 10(b) have exactly the same count rate.

TABLE II.- COMPARISON OF THE CALCULATED POISSON AND THE MEASURED DISTRIBUTION

h	$P_n = \frac{1}{n!} e^{-1}$	Measured
0	0.368	0.38
1	.368	.34
2	.184	.21
3	.0613	.06
4	.0153	.01
>4	.0034	0
$\sum$	1.000	1.00

Note: The agreement between the calculated Poisson distribution and the measured distribution is remarkably close.

TABLE III.- PROBABILITY CALCULATION FOR DETECTING A PARTICLE

(for $n = 70$, $y = 3$)

X	P(x)	$P(N > y/x)$	$P(x)P(N > y/x)$
0-2	0.055	0	0
3	.045	.125	.0056
4	.068	.313	.0214
5	.115	.500	.0575
6	.147	.656	.0962
7	.158	.773	.1220
8	.147	.855	.1260
9	.115	.910	.1050
10	.068	.945	.0640
11	.045	.961	.0430
12	.022	.980	.0215
13	.013	.989	.02128
14	.001	.994	.0010
> 14	Negligible		$\sum = .676$

The square of this sum $(0.676)^2$ is the probability that both screens will "see" the particle. To show the trend, three more points were calculated and are entered in table IV.

TABLE IV.- PROBABILITY OF DETECTING A PARTICLE FOR GIVEN n AND y

Number of photons arriving at the photocathode	n = 70	n = 100
y = 2	$(0.84)^2 = 0.70$	$(0.92)^2 = 0.85$
y = 3	$(0.68)^2 = 0.46$	$(0.86)^2 = 0.74$

TABLE V.- PERMISSIBLE NOISE PULSE RATES

	1 error / week	1 error / month
Two electrons counted as an event	380	266
Three electrons counted as an event	6910	3280

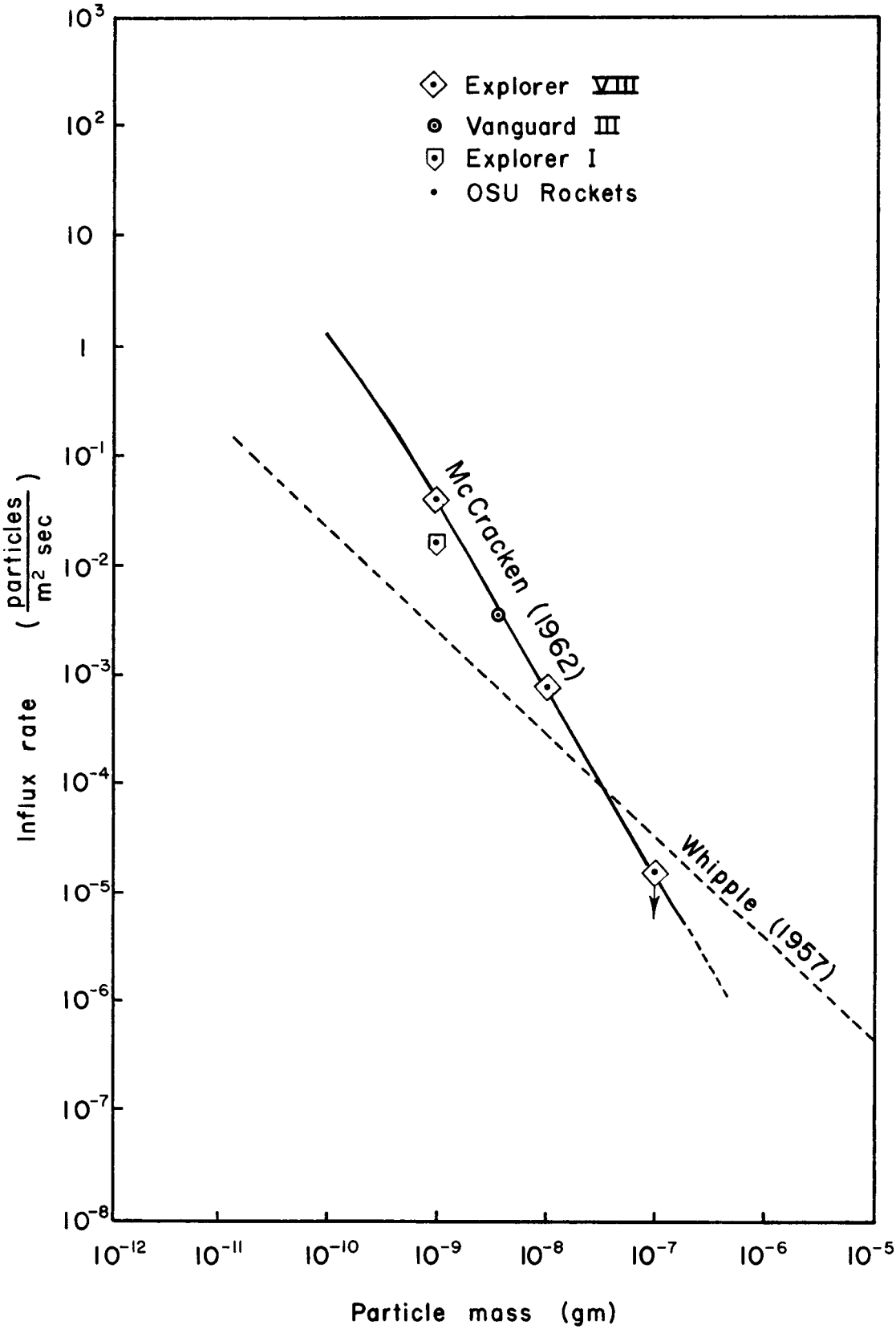

Figure 1.- Distribution curve for interplanetary dust particles in the vicinity of earth.

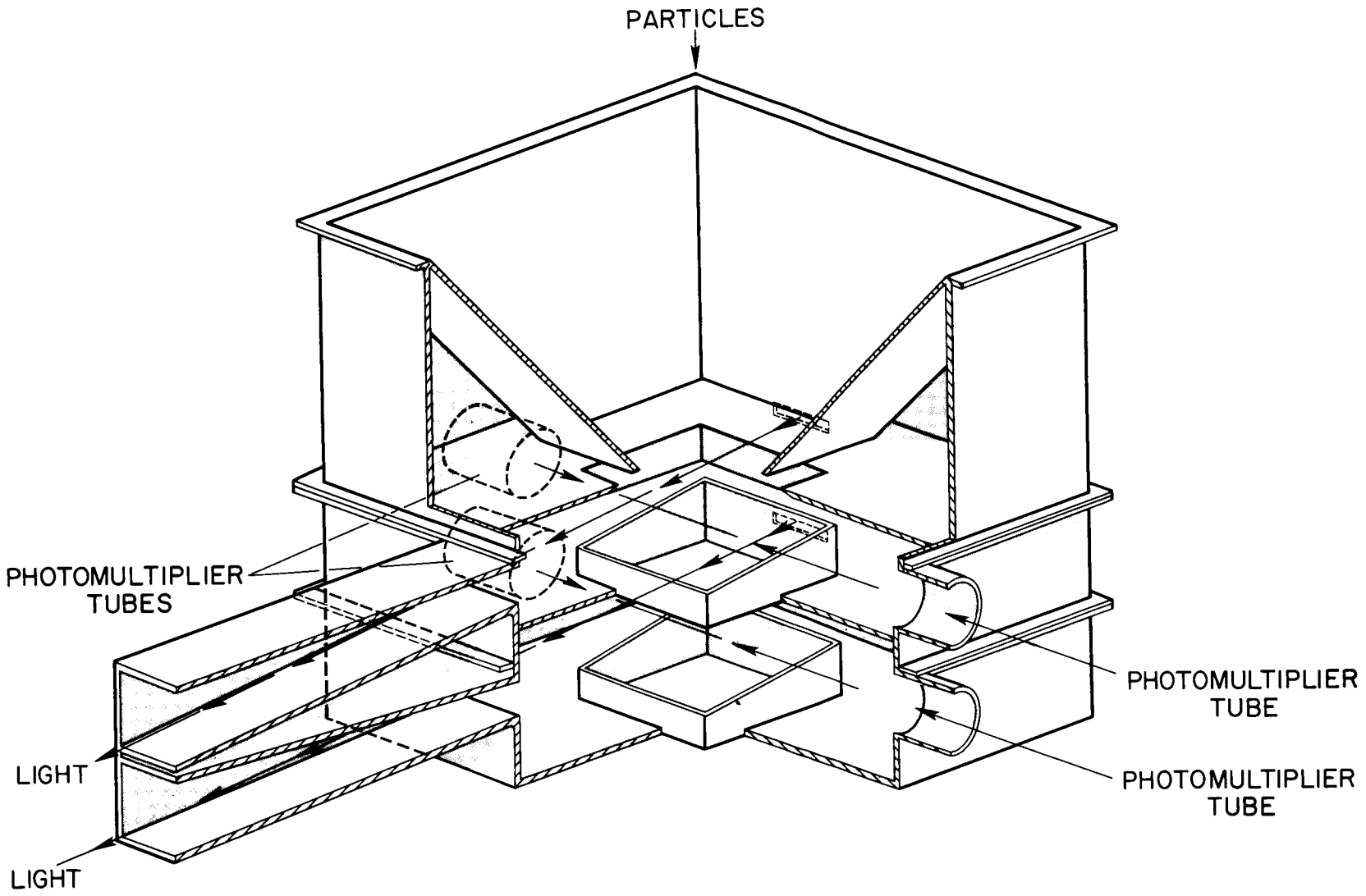

Figure 2.- Physical construction of the micrometeoroid velocity detector.

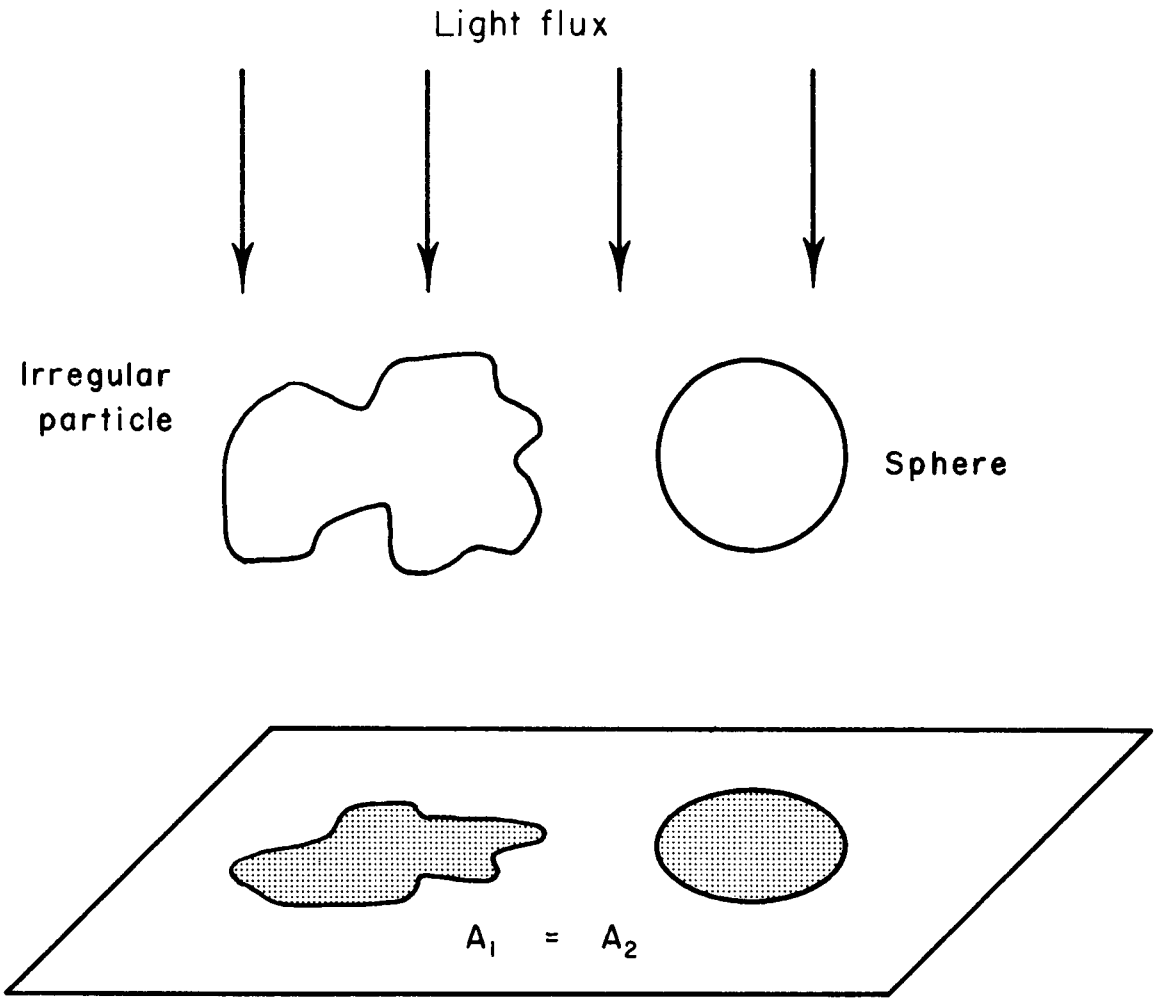

Figure 3.- Definition of the equivalent particle radius.

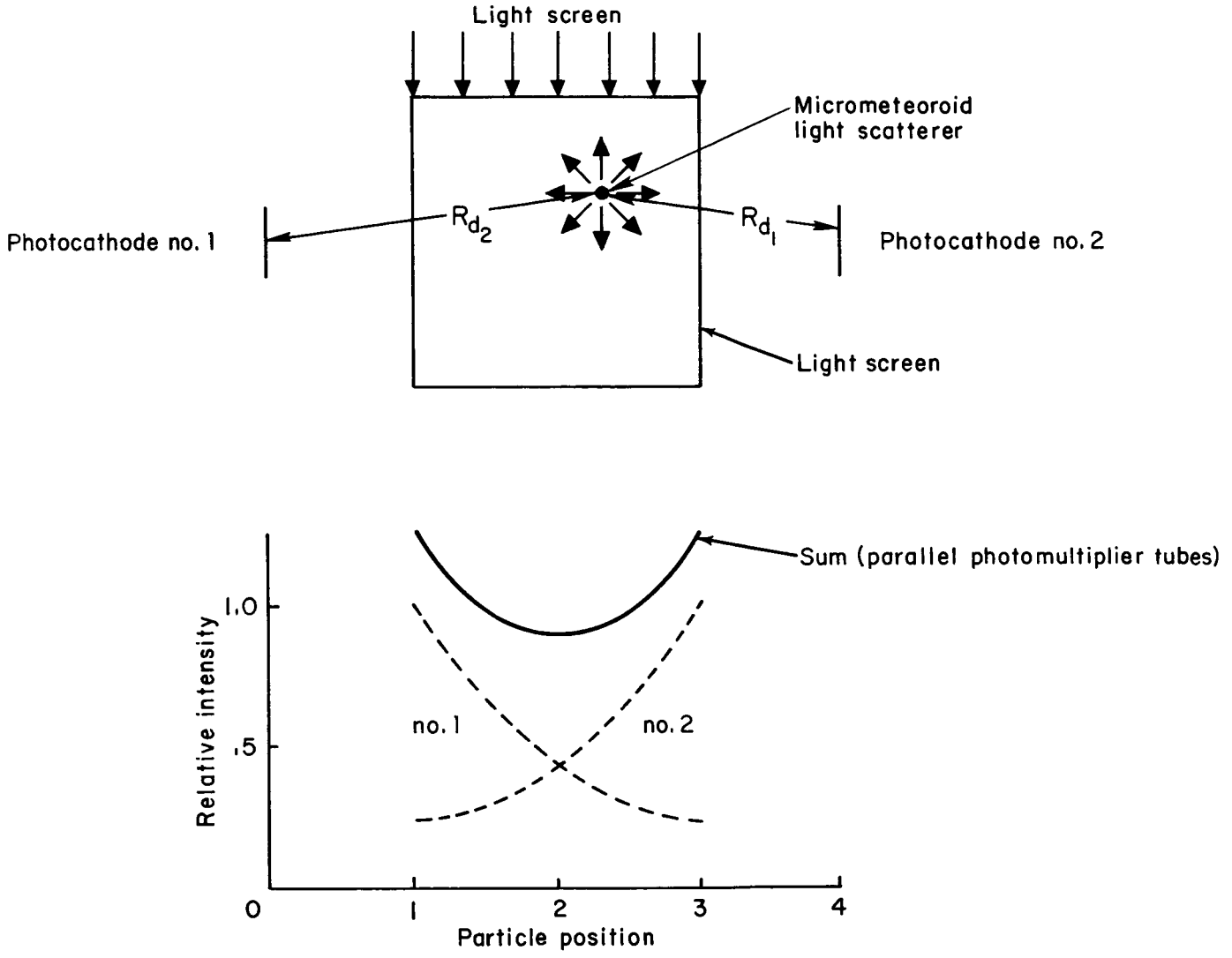

Figure 4.- Detector sensitivity as a function of the particle position in the light screen.

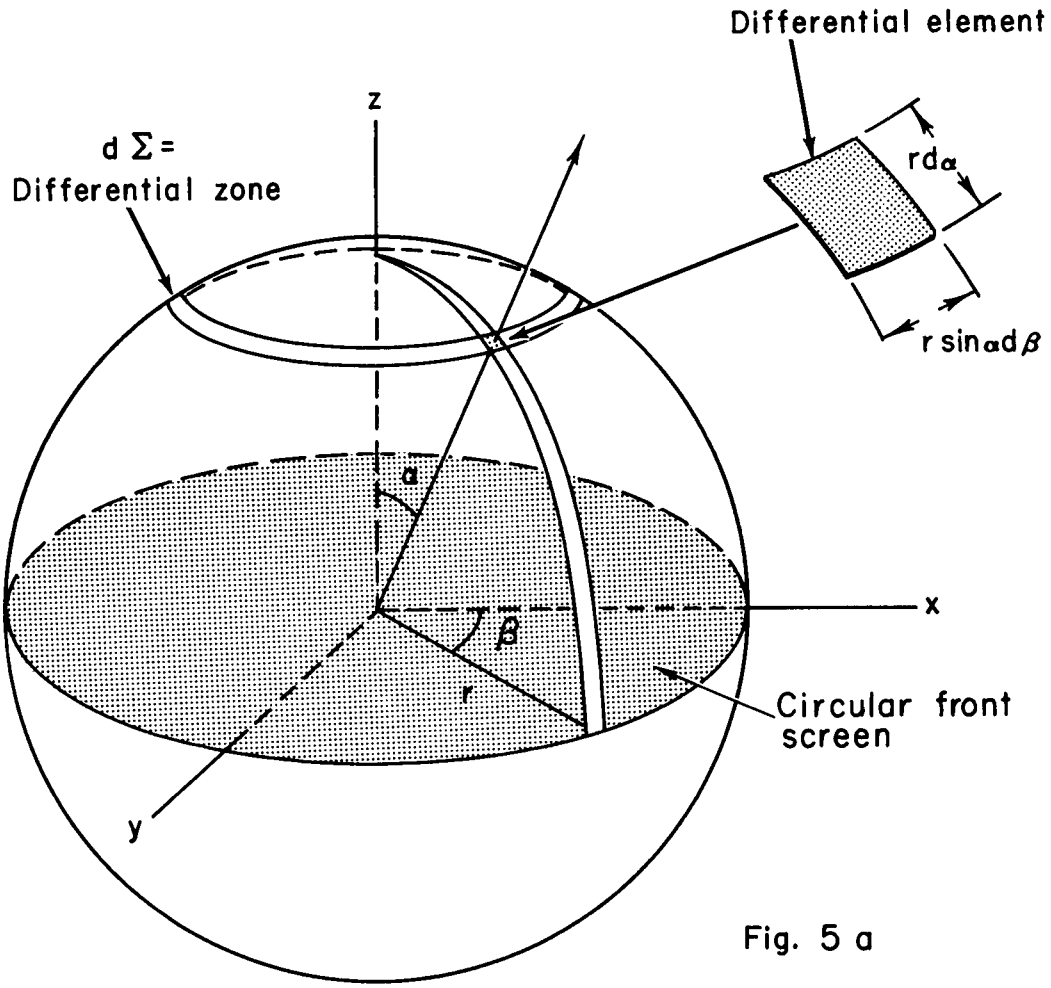

Fig. 5 a

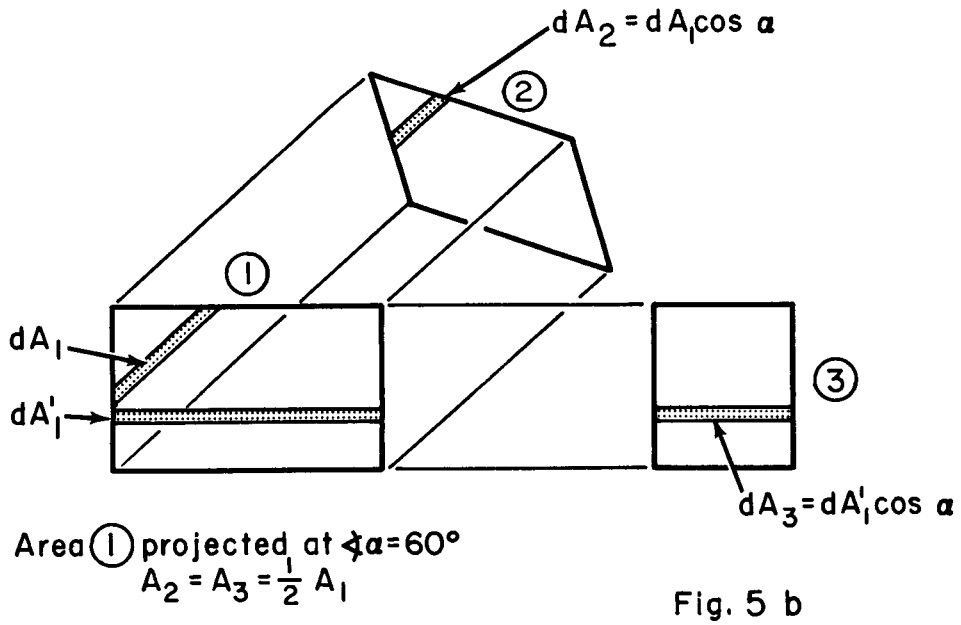

Fig. 5 b

Figure 5.- Coordinates for calculating the relative front window size.

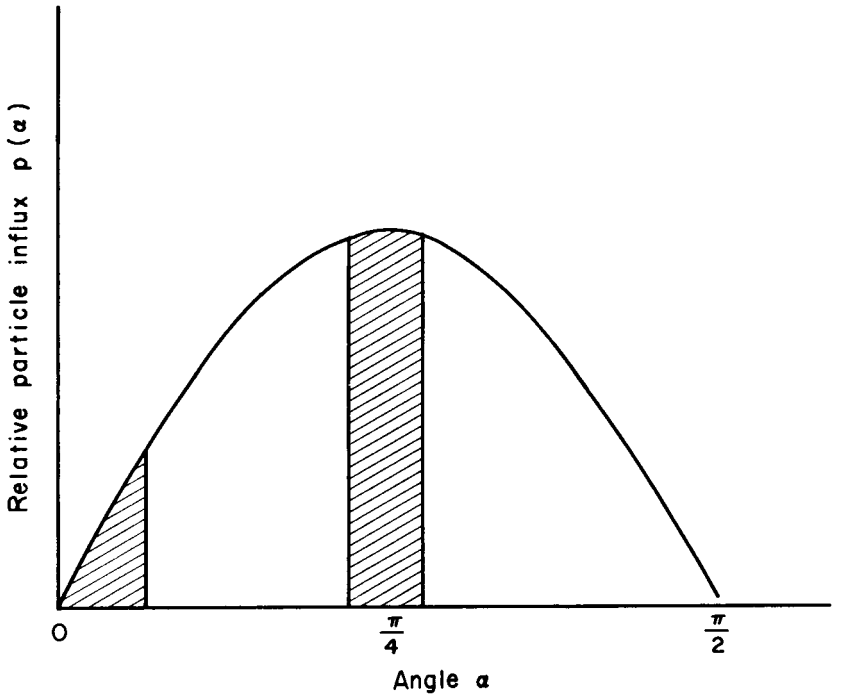

Figure 6.- Probability density function of the relative particle influx.

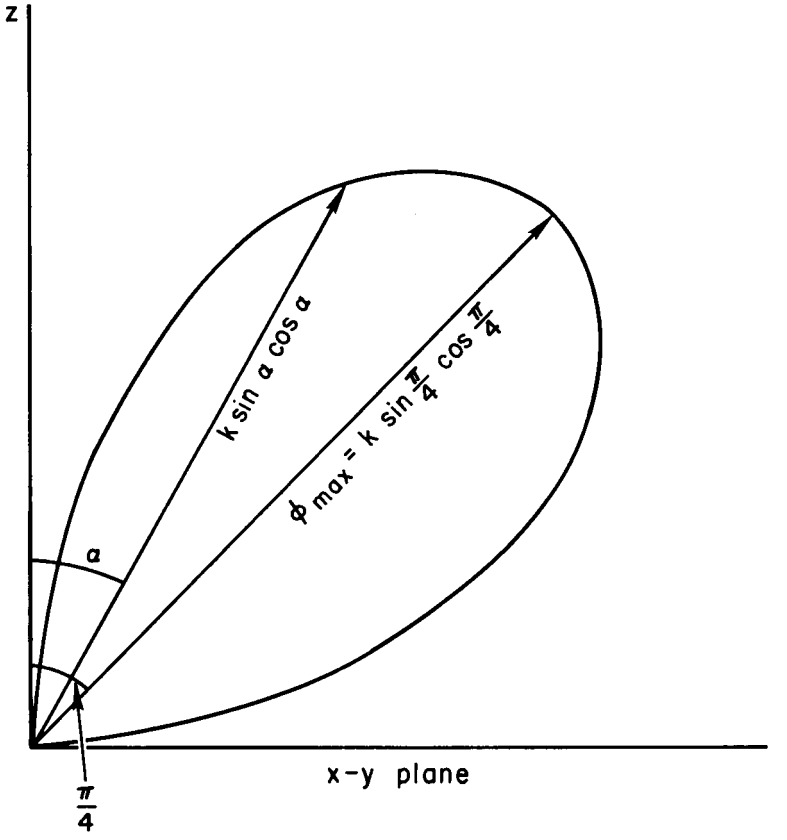

Figure 7.- Relative flux intensity in polar coordinates.

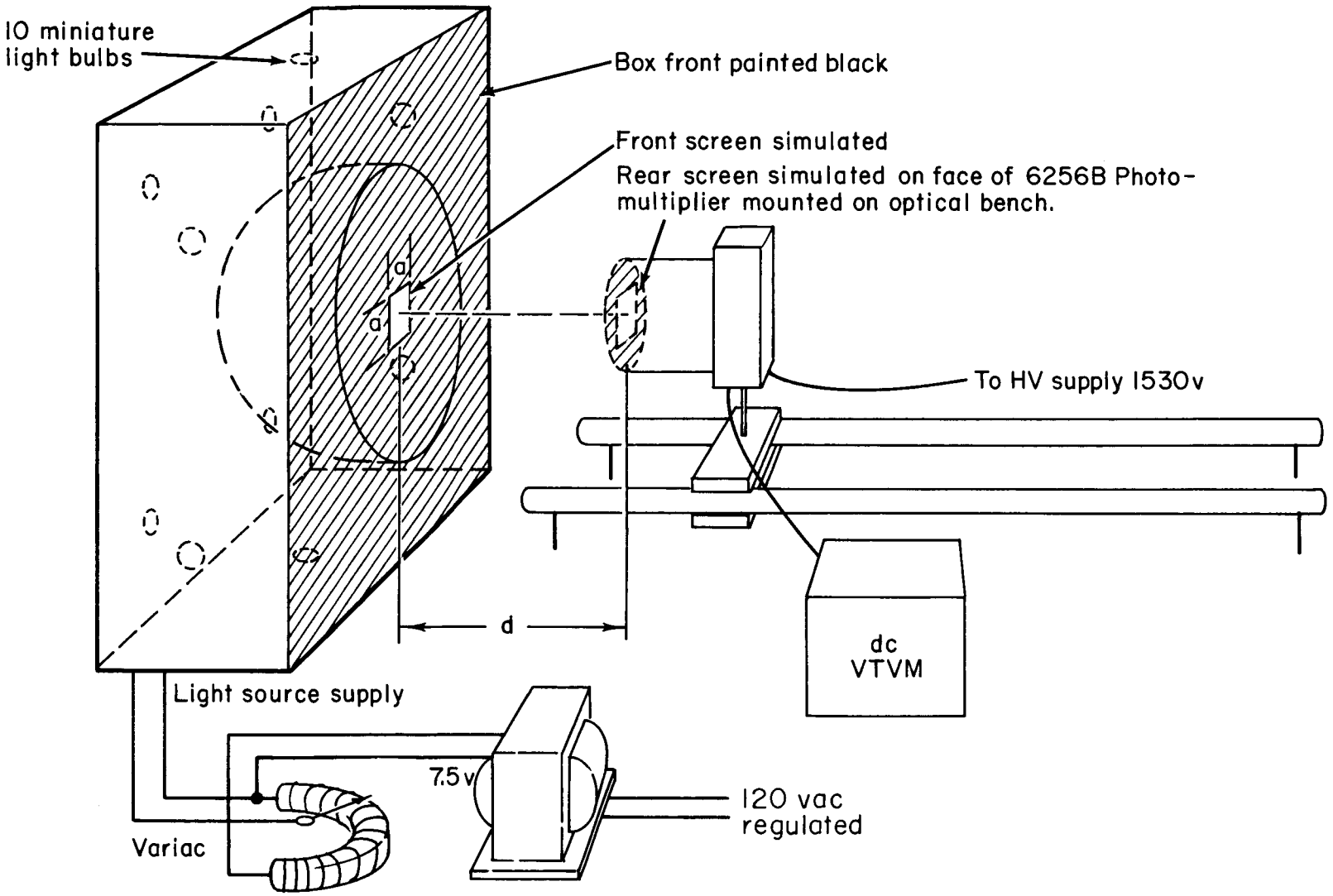

Figure 8.- Test setup for coincidence ratio measurement performed in a dark room.

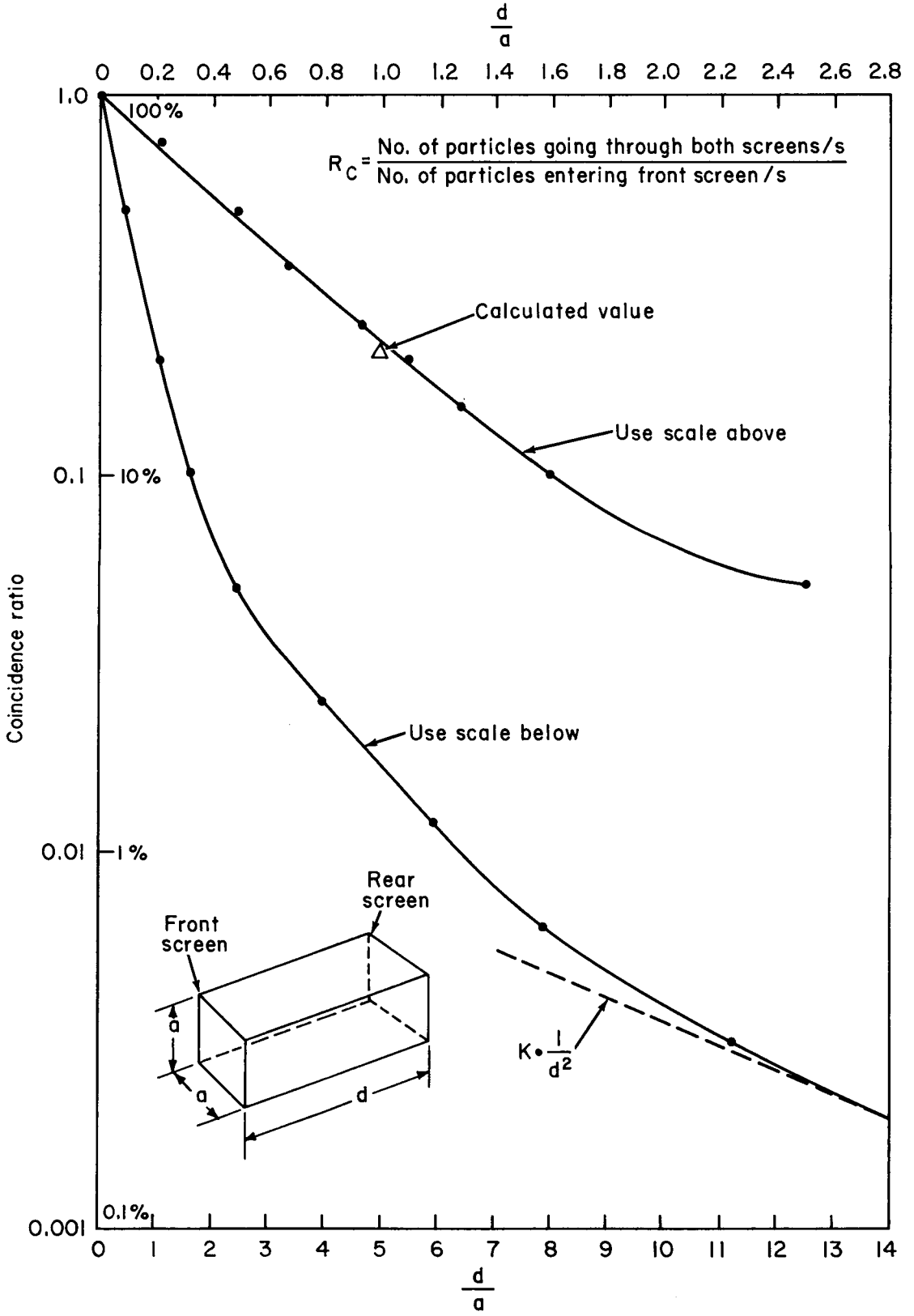

Figure 9.- Measured coincidence ratio.

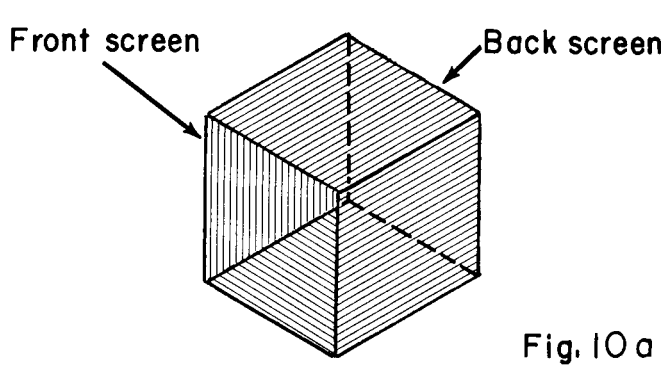

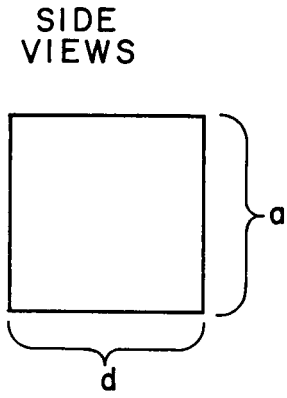

Fig. 10 a

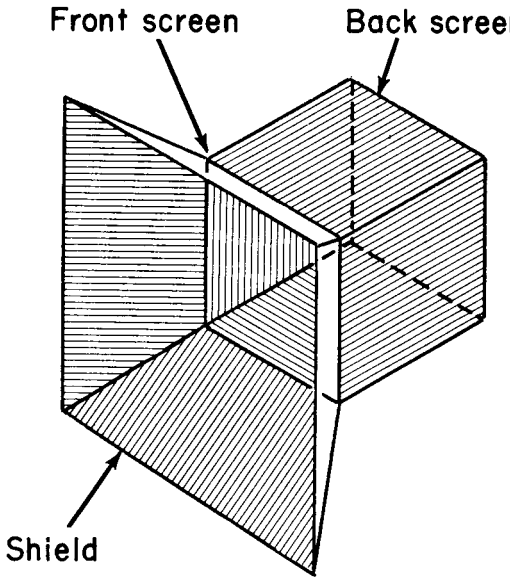

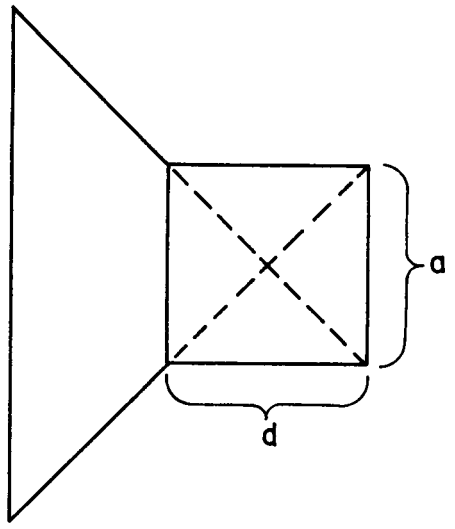

Fig. 10 b

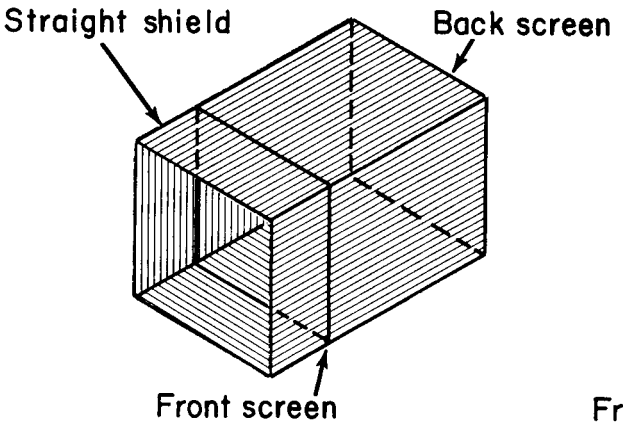

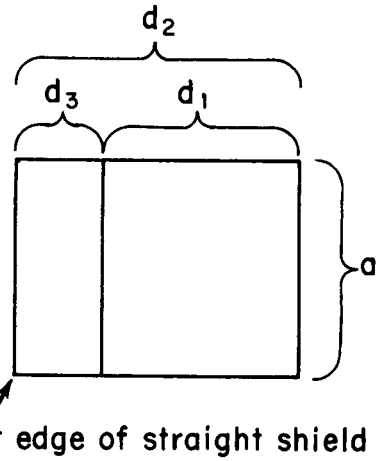

Figure 10.- Possible detector geometries.

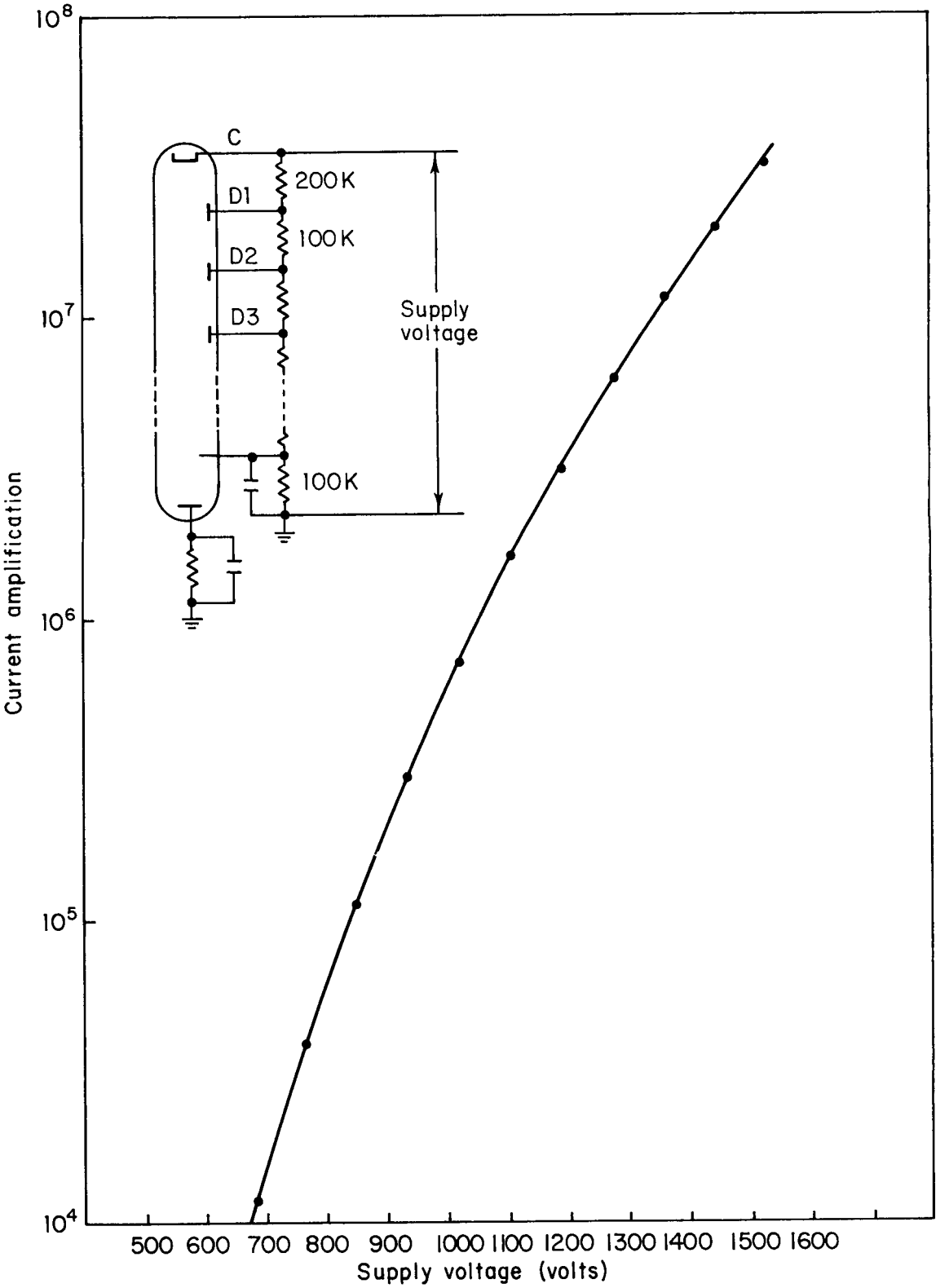

Figure 11.- Measured current gain of the EMI9502B photomultiplier tube.

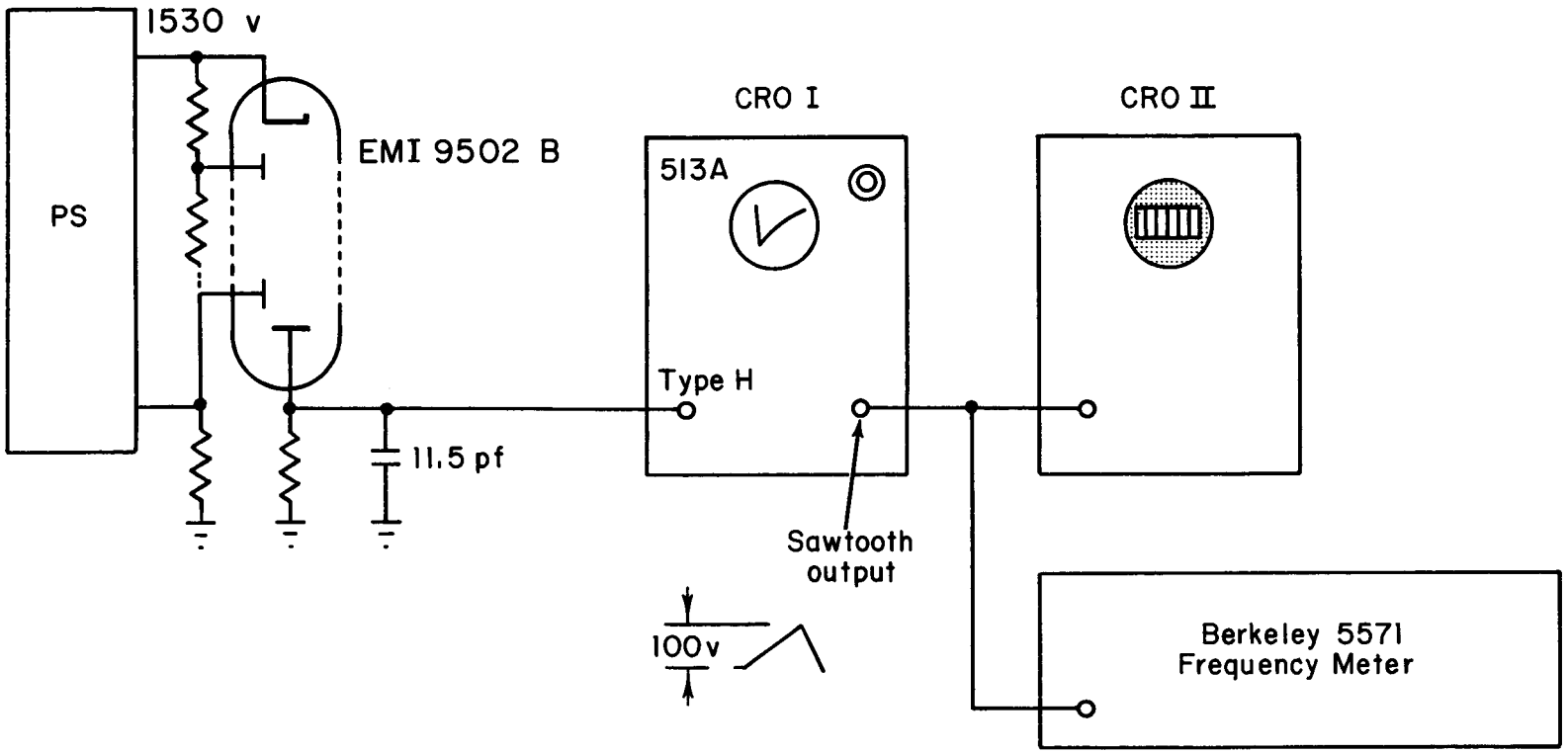

CRO I 1) Adjust trigger for minimum level to be included in the counting. (Changing horizontal sensitivity by a certain factor will increase trigger level by the same factor).

2) Adjust stability control as far to the right as possible for still stable triggering.

3) Adjust attenuator on counter to 10 to get proper count rate.

Figure 12.- Pulse time distribution and height analysis circuit.

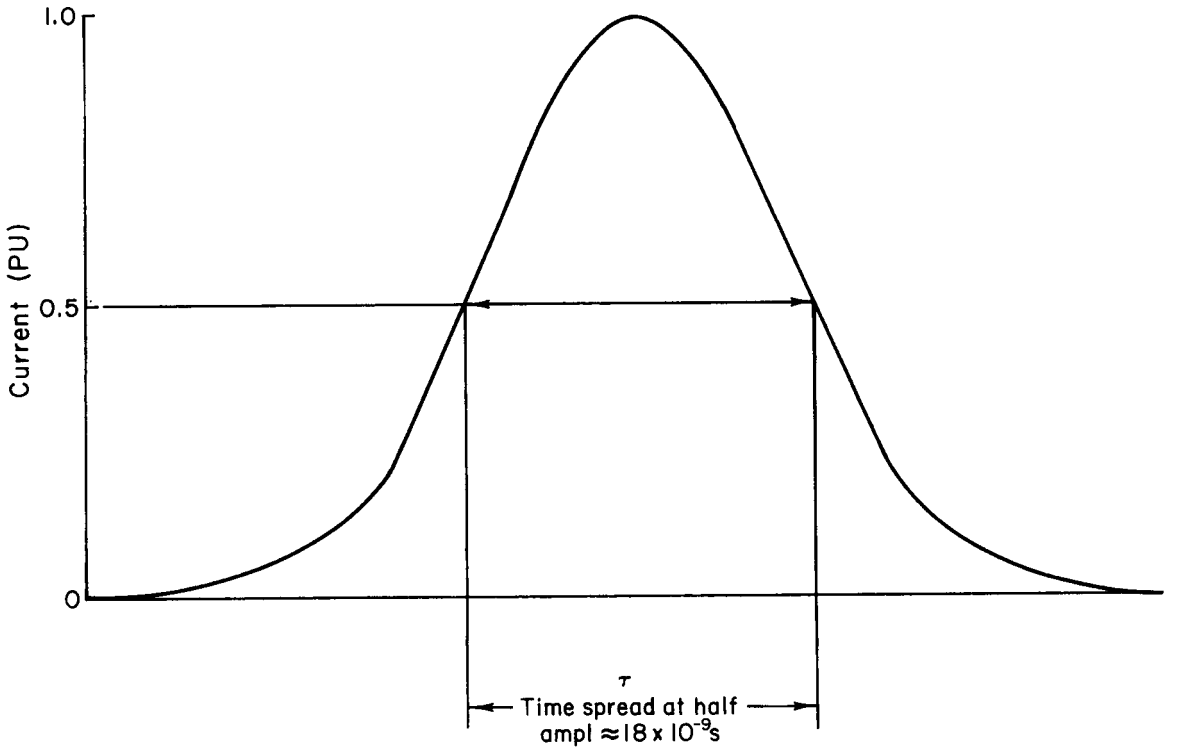

Figure 13.- Gaussian current pulse.

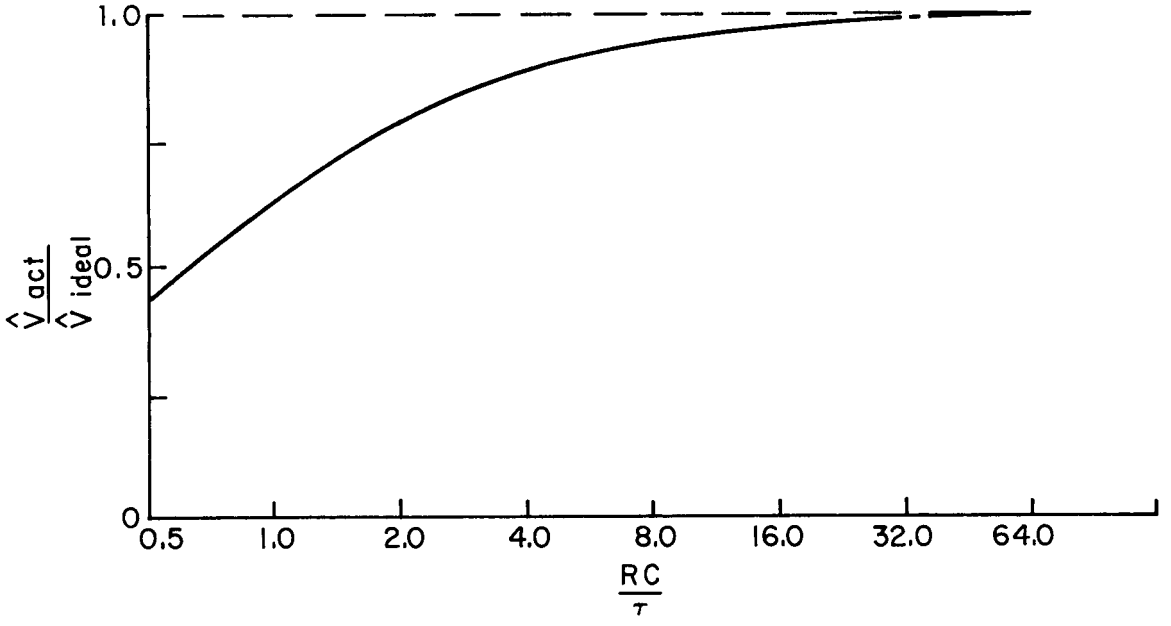

Figure 14.- Calculated pulse height for different load impedances.

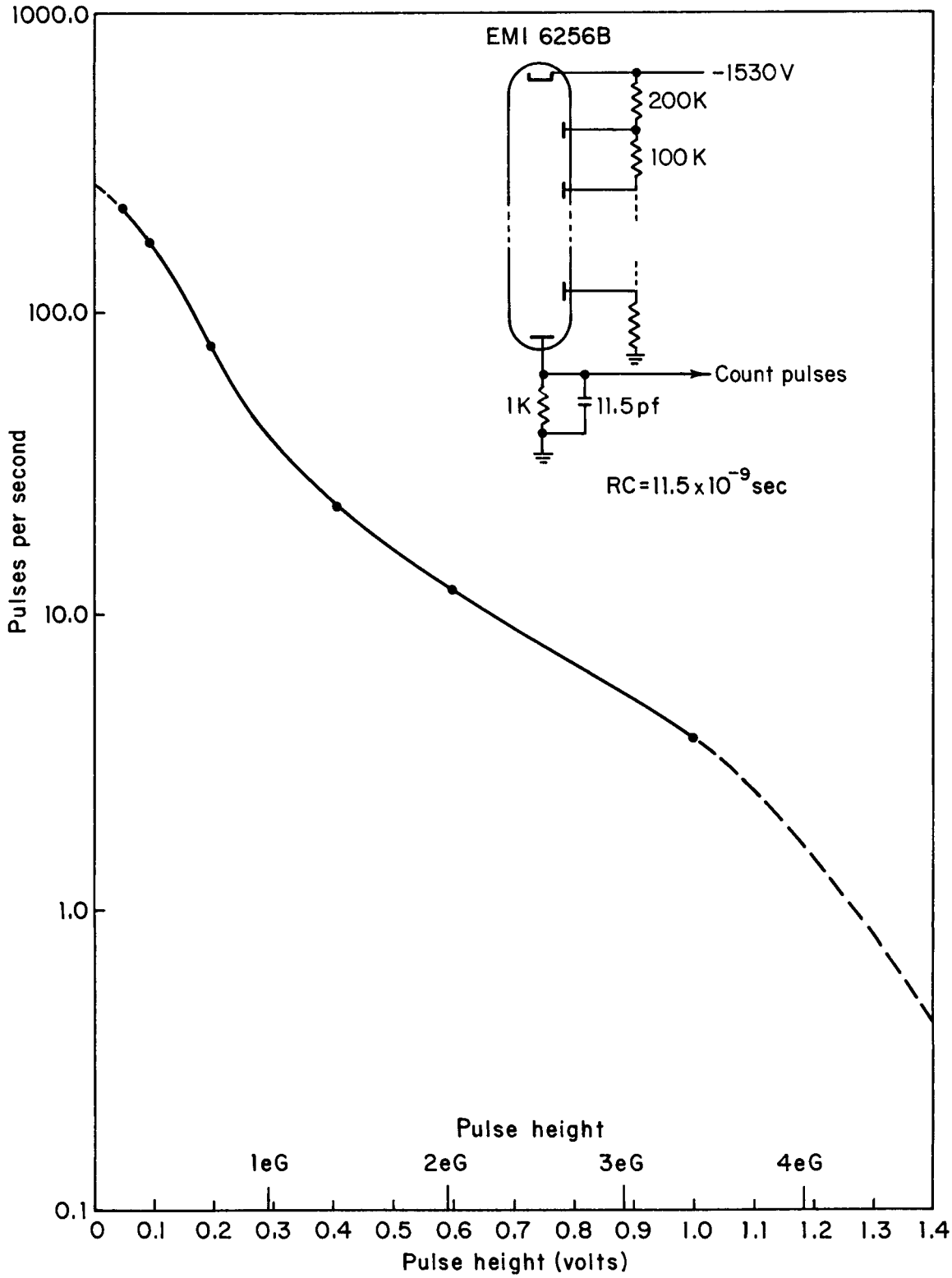

Figure 15.- Number of pulses greater than a given pulse height versus minimum pulse height.

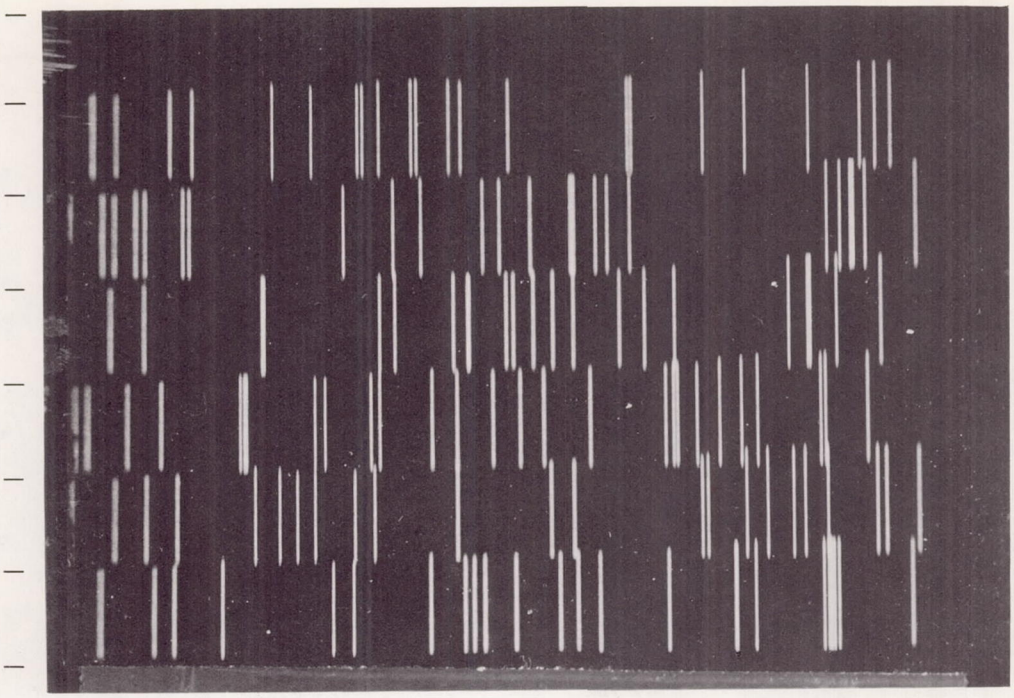

Figure 16.- Pulse time distribution.

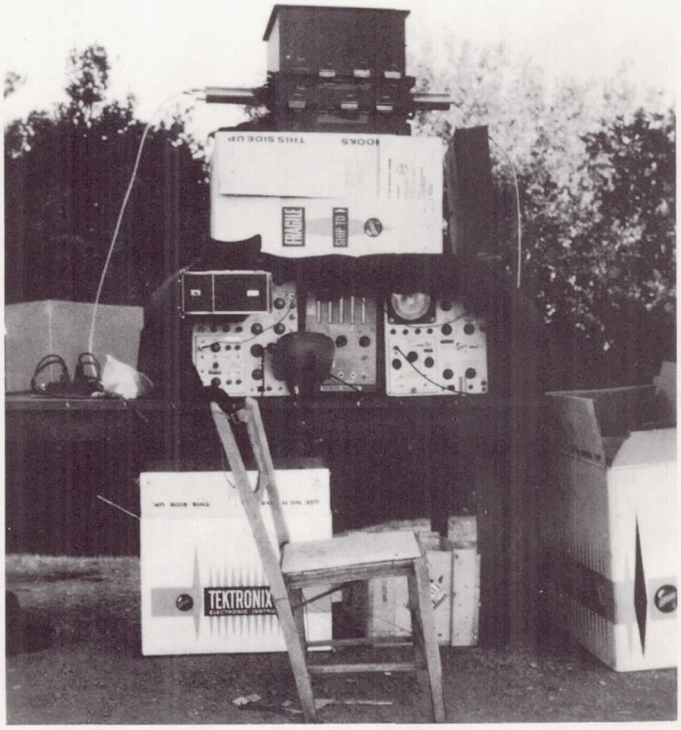

Figure 17.- Test setup at Mt. Hamilton.

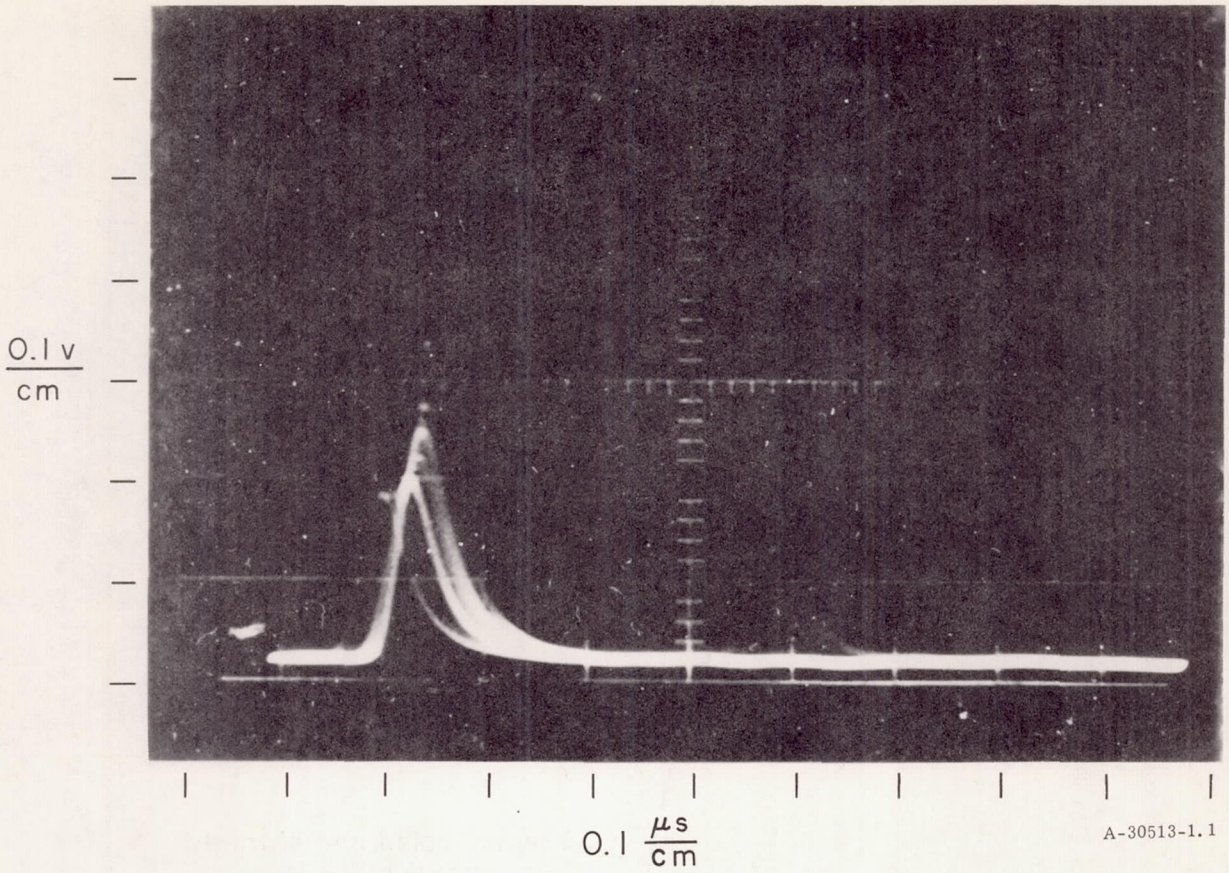

Figure 18.- Pulse shapes of the photomultiplier tube output due to starlight and thermal noise.

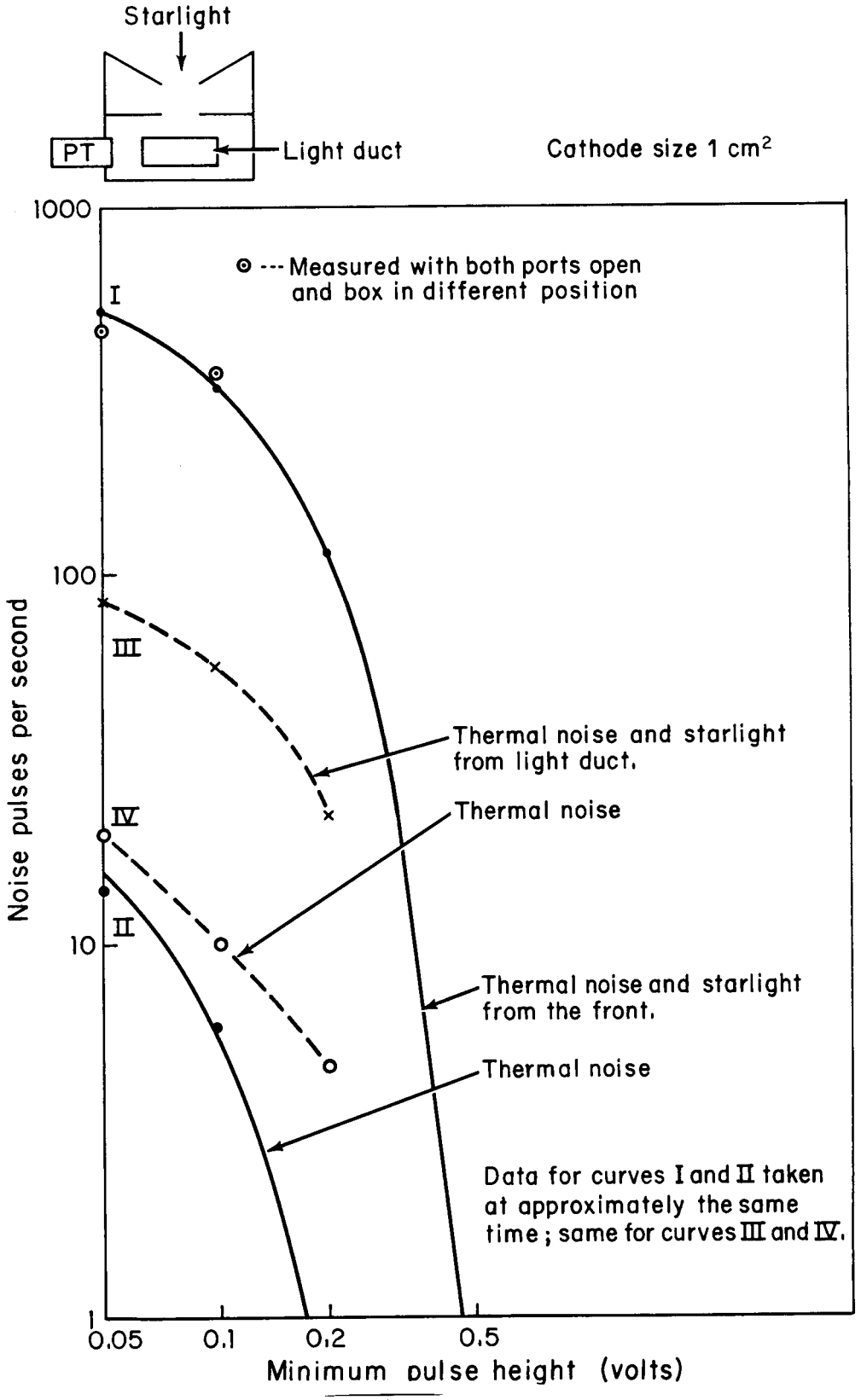

Figure 19.- Phototube noise due to starlight and thermal noise using EMI9502B.

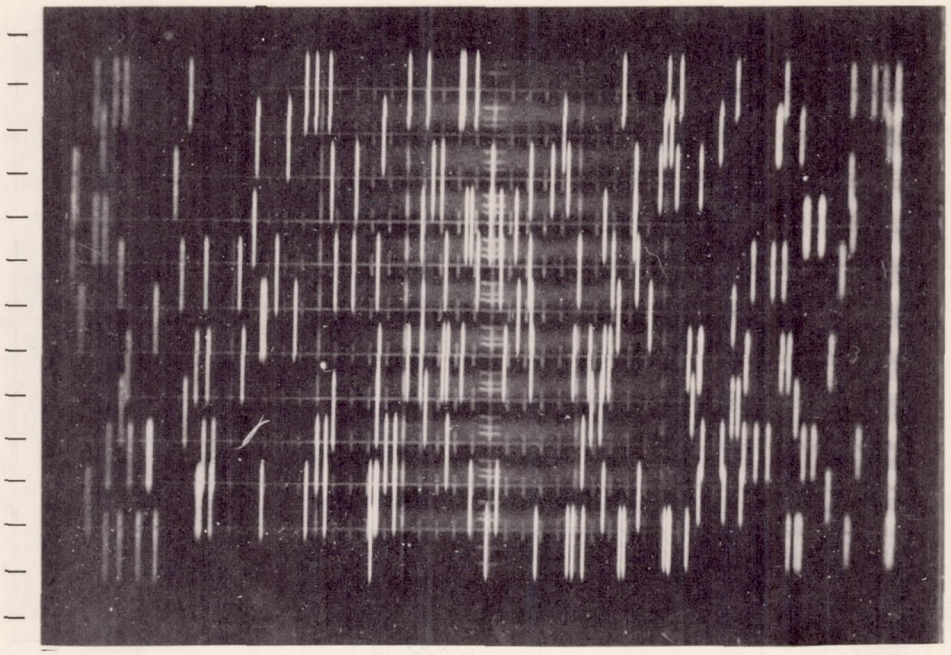

Figure 20.- Pulse time distribution of photomultiplier tube output due to starlight and thermal noise.

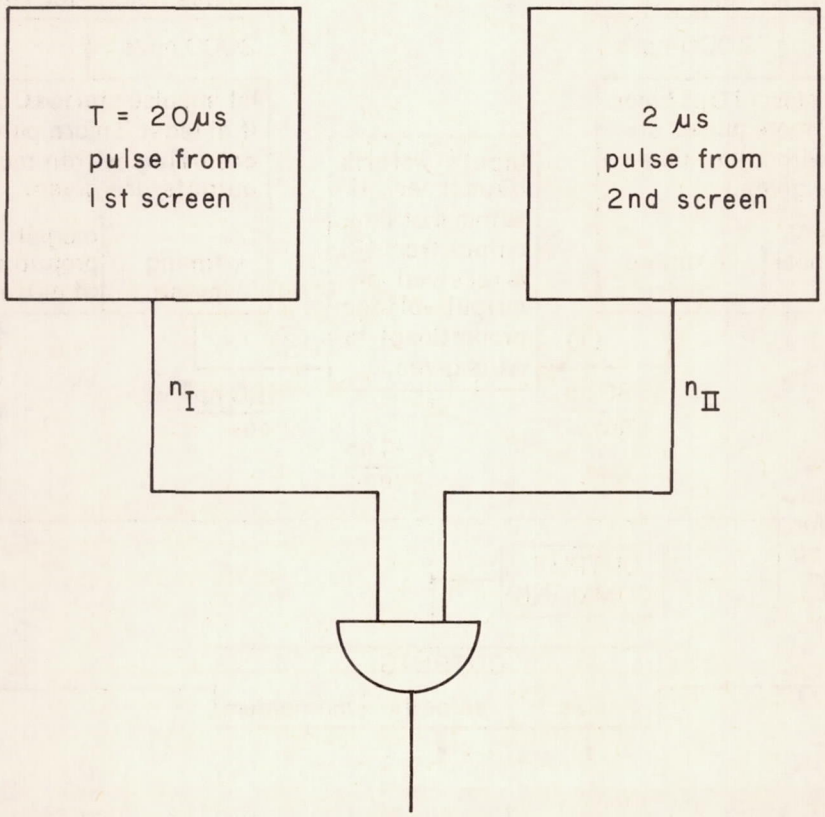

Figure 21.- Coincidence gate for two outputs.

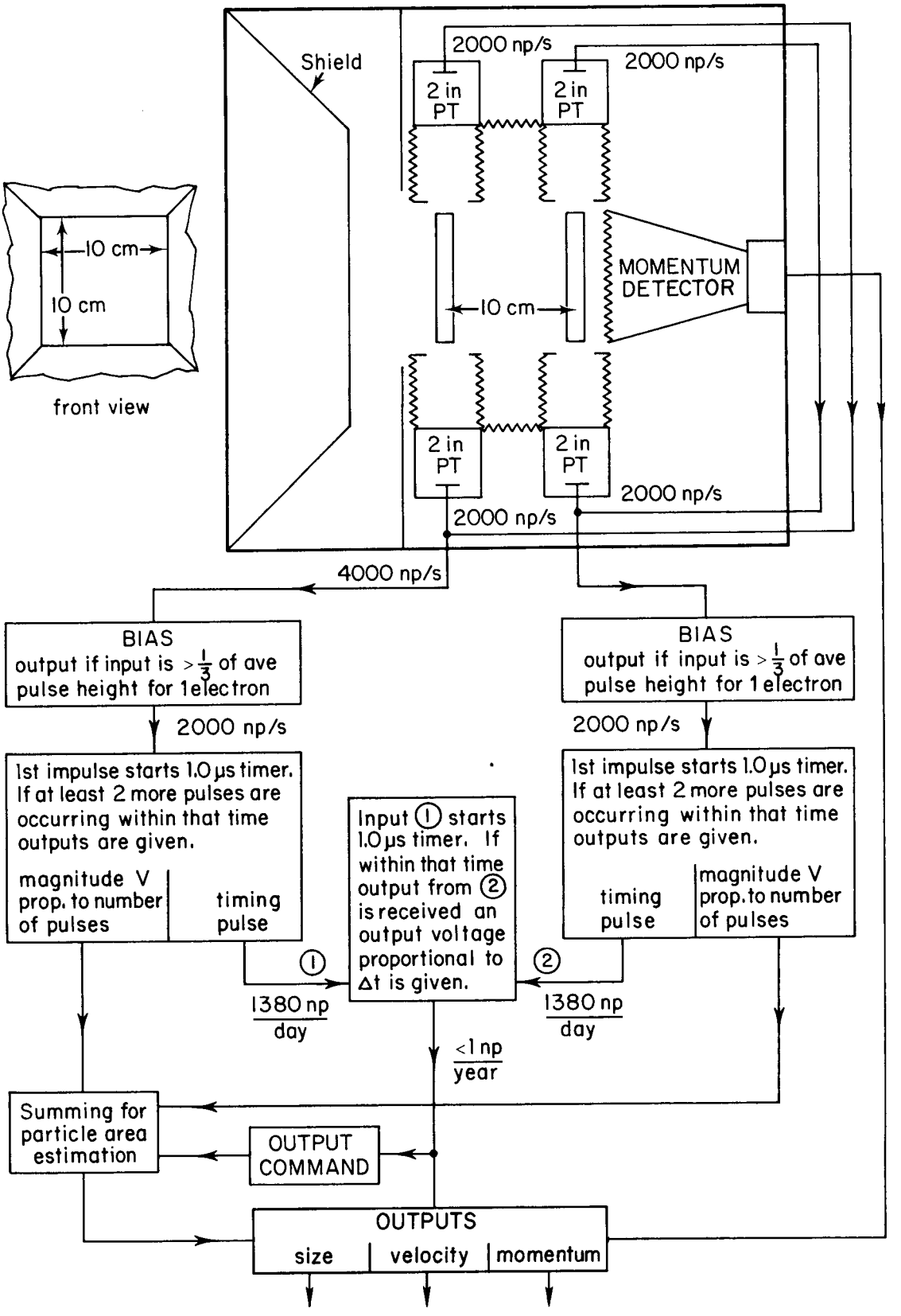

Figure 22.- Block diagram of the velocity detector.